



# *Azadirachta indica* peel extract-mediated synthesis of ZnO nanoparticles for antimicrobial, supercapacitor and photocatalytic applications

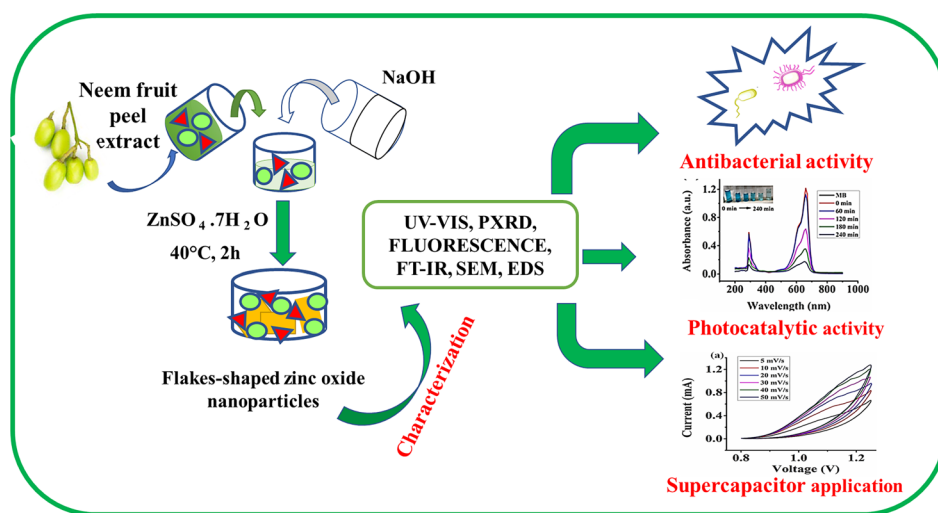
Nutan Rani<sup>1</sup> · Sapna Yadav<sup>1</sup> · Asifa Mushtaq<sup>2</sup> · Swati Rani<sup>3</sup> · Mona Saini<sup>1</sup> · Seema Rawat<sup>4</sup> · Kalpna Gupta<sup>5</sup> · Kalawati Saini<sup>1</sup> · Dipak Maity<sup>6</sup>

Received: 19 September 2023 / Accepted: 20 January 2024 / Published online: 22 February 2024  
© The Author(s), under exclusive licence to the Institute of Chemistry, Slovak Academy of Sciences 2024

## Abstract

In this work, flake-shaped zinc oxide (ZnO) nanoparticles (NPs) labeled as (P3) are green synthesized using *Azadirachta indica* fruit peel extract for antibacterial, supercapacitor, and photocatalytic applications. XRD pattern revealed the hexagonal wurtzite crystalline structure of the green synthesized ZnO NPs while FTIR spectrum confirmed their surface-attached phytochemicals coating. FE-SEM image demonstrated micro to nano-sized flake-shaped ZnO NPs with widths 116–145 nm and lengths 215–398 nm. The surface area of synthesized ZnO NPs was obtained as 22.721 m<sup>2</sup>/g using Brunauer–Emmett–Teller (BET) analysis. Minimum inhibitory concentration (MIC) values of as-prepared ZnO NPs are determined as 140, 135, and 130 µg/mL against *Escherichia coli*, *Pseudomonas aeruginosa*, and both *Staphylococcus aureus* and *Streptococcus pneumoniae*, respectively. Moreover, as-synthesized ZnO NPs showed high specific capacitance and energy density values of 794.96 F/g and 22.34 Wh/kg at 5 mV/s, respectively. Furthermore, as-prepared ZnO NPs showed 88.53% and 83.08% photocatalytic degradation for methylene blue and rhodamine B dye, respectively, after 240 min of sunlight exposure. In summary, green synthesized flake-shaped ZnO NPs are promising candidates for antibacterial, supercapacitor, and photocatalytic applications.

## Graphical abstract



**Keywords** Green synthesis using plant extract · Zinc oxide nanoparticles · Antimicrobial activity · Supercapacitor · Photocatalytic degradation

## Introduction

Nowadays, metal oxide nanoparticles (MONPs)-based nanotechnology has vastly increased, particularly in biomedical, water purification, supercapacitors, pharmaceuticals, and sensors. Recently many biocompatible MONPs have been synthesized by plant extracts rather than utilizing conventional techniques such as chemical-reduction wet method, hydrothermal method, sol–gel, laser ablation, ball milling, microwave-assisted, and many other methods. Various research articles are reported in the literature where green synthesized ZnO NPs have been studied for their in vitro and in vivo cytotoxic activity. Among various metal oxide nanoparticles (MONPs), zinc oxide (ZnO) nanoparticles (NPs) have been widely explored in biomedical (Saini et al. 2022a, b, c; Rabiee et al. 2022), supercapacitor (Rani et al. 2020), UV-absorber (Becheri et al. 2008), biosensor (Umar et al. 2009), photoluminescent (Madan et al. 2016), photocatalytic (Rokhsat and Akhavan 2016; Khan et al. 2021; Saini et al. 2022a, b, c), optoelectronic (Harun et al. 2017), and antibacterial (Jones et al. 2008) applications because of their high chemical/thermal stability (Bijanazad et al. 2015) and unique physicochemical properties (Akhavan 2010).

Plant extract-mediated green synthesis of MONPs has received a great deal of attention as different plant parts consist of various phytochemicals (nimbin, nimbolinin, nimbidol, nimbidin, gedunin, sodium nimbin, quercetin, salannin, etc., have been reported in different parts of neem tree) which can simultaneously act as reducing and stabilizing agents. An essential limonoid called gedunin is found predominantly in seeds and different genera of the Meliaceae family. Koumaglo et al reported that the concentration of gedunin is maximum in the green fruit epicarp compared to the ripened fruit (Koumaglo et al. 2004). Green synthesized nanoparticles are biocompatible and exhibit less toxicity. Hence these biosynthesized ZnO nanoparticles can be utilized for biomedical applications. Besides, extracts of medicinal plants (such as *Azadirachta indica*) consisting of phytochemicals have huge potential to be used for several biomedical applications due to their antimicrobial (i.e., antibiotics, antivirals, antifungals, and antiparasitic), antitumor, antioxidant, anti-protozoal, antiarthritic, antiseptic, antipyretic, anti-inflammatory, anti-ulcer properties (Srivastava et al. 2020). Currently, green synthesized ZnO NPs have been extensively studied due to their synergic effects on antimicrobial (Mohammadi-Aloucheh et al. 2018; Bala et al. 2015; Huang et al. 2008), antifungal (Noohpishaha et al. 2020), antidiabetic (Rani et al. 2022a, b, c; Arvanag et al. 2019), anticancer (Rani et al. 2022a, b, c; Soltanian et al. 2021; Li et al. 2021; Ray et al. 2019) and photocatalytic activities

(Mashentseva et al. 2022) besides biocompatibility and less toxicity (Visinescu et al. 2018). For example, *Cassia auriculata* leaf extract-mediated biosynthesized ZnO NPs have been explored to enhance antibacterial as well as anticancer activities (Padalia et al. 2018). Likewise, *Trifolium pratense* flower extract-mediated green synthesized ZnO NPs have been investigated as antimicrobial agents (Dobrucka and Dugaszewsk 2016). Similarly, Prashanth et al. (2015) reported biosynthesis of ZnO NPs using aqueous fruit extracts of *Punica granatum* L. and *Tamarindus indica* L. for antimicrobial applications.

In recent times, the development of highly efficient nanomaterials (NMs) based supercapacitors is in serious demand to effectively replace the conventional dielectric materials-based electrostatic capacitors of energy storage devices (Handayani et al. 2022; Ehsani et al. 2022). MONPs (n-type semiconductors) have shown great promise as supercapacitors because of their large surface-to-volume ratio, high energy density, and long cyclic life (Nagarani et al. 2022; Sinha et al. 2022). Recently, ZnO NPs have been widely investigated as supercapacitors due to their strong electrochemical activity and direct band gap of 3.37 eV (Yadav et al. 2022a, b; Buldu-Akturk et al. 2022). Mohan et al. have demonstrated a high specific capacitance of 133 F/g at 10 mV/s for Ni-doped ZnO NPs (Mohan et al. 2022). Nethaji and Kumar (2022) have also reported  $V_{0.07}Ag_{0.07}ZnO$  nanorods with an enhanced specific capacitance of 2700.19 F/g at 5 mV/s. Similarly, Choubari et al. (2022) have revealed a specific capacitance of 431 F/g for green synthesized  $CeO_2/ZnO$  nanocomposite. Likewise, Moghadam and Seif (2022) have exhibited a specific capacitance of 523 F/g at 10 mV/s for  $ZnO/CNT/Fe_3O_4/Ni$  foam nanocomposite.

In the last few decades, the photocatalytic dye degradation approach has gained considerable attention for the removal of toxic organic dyes present in industrial wastewater as it is facile, inexpensive, and eco-friendly compared to various other techniques like activated carbon adsorption, aerobic biodegradation, membrane filtration and adsorption, liquid–liquid extraction (Yadav et al. 2022a, b). Among various nanomaterials, MONPs with suitable band gap energy have been widely investigated as photocatalysts for organic dye degradation. For example, 89.88% degradation of methylene blue (MB) dye using  $NiO/Co_3O_4$  nanocomposite has been reported under sunlight irradiation (Yadav et al. 2022a, b). Analogously, 88.46% and 93.63% degradation of crystal violet (CV) and MB dyes have been revealed under sunlight exposure using  $NiO/Cr_2O_3$  nanocomposite (Yadav et al. 2022a, b). Likewise, ZnO NPs have been exploited as photocatalysts for 96%, 69%, and 48% degradation of malachite green (MG), MB, and methyl orange (MO), respectively, under ultraviolet light irradiation (Asha et al. 2022). Similarly, ZnO/bentonite nanocomposite exhibited 95% photocatalytic degradation of MB dye (Golmohammadi et al. 2022).

Though green synthesized ZnO NPs have been studied extensively for various applications, but their antimicrobial, supercapacitance, and photocatalytic effects are not explored by any research group. In this work, we have reported *Azadirachta indica* fruit peel extract-mediated green synthesis of ZnO NPs and evaluated their potential as an antibacterial agent, photocatalyst, and supercapacitor. The antibacterial potential of phytochemicals coated green synthesized ZnO NPs is investigated against *Pseudomonas aeruginosa*, *Escherichia coli*, *Staphylococcus aureus*, and *Streptococcus pneumoniae* while explaining possible mechanism for the antibacterial activity. Moreover, photocatalytic activities of as-synthesized ZnO NPs are examined for photocatalytic degradation of MB and rhodamine B (RhB) dyes under sunlight irradiation. Finally, their electrochemical performance is investigated for enhanced supercapacitor application. Furthermore, antimicrobial, electrochemical, and photocatalytic dye degradation activities of as-synthesized ZnO NPs are compared with reported green synthesized ZnO NPs.

## Materials and methods

### Materials

ZnSO<sub>4</sub>·7H<sub>2</sub>O (Zinc sulfate heptahydrate), NaOH (Sodium hydroxide), Methylene Blue, and Rhodamine B were purchased from Central Drug House (P) Ltd—CDH, India. KOH (Potassium hydroxide) was received from Avantor Performance Materials India Limited. Commercialized ZnO (CAS- 1314-13-2, EC- 215-222-5, purity-99.9%) and Nafion (AR grade) were purchased from Sigma-Aldrich Co. 3050 Spruce Street, St. Louis, MO 63103 USA. All the chemicals were analytical reagent grade.

### Preparation of *Azadirachta indica* fruit peel extract

*Azadirachta indica* fruits were collected from the Department of Chemistry, University of Delhi, New Delhi-110007, India. Peels of these fruits were removed and washed with double distilled water. The washed peels were dried in a hot air oven for 2 h at 60 °C and then ground into powder. Next, a 25% (w/v) aqueous solution of the peel powder was prepared and then heated at 40 °C with continuous stirring for half an hour. Finally, an aqueous solution of peel extract was filtered through a Whatman paper.

### Green synthesis of ZnO NPs

50 mL aqueous solution (0.2 M) of ZnSO<sub>4</sub>·7H<sub>2</sub>O and 50 mL aqueous solution of NaOH (2.0 M) were taken in a 250 mL conical flask. 3 mL of freshly prepared 25% (w/v) *Azadirachta indica* fruit peel extract was added into the flask

and magnetically stirred at room temperature for 30 min. Then, the mixture solution was heated to 40 °C and kept at that temperature for 2 h under constant stirring (400 rpm) using a hot plate magnetic stirrer. Afterward, the resulting precipitates of NPs were washed with 90% alcohol followed by centrifugation several times. One-half of the washed NPs (P3) were suspended in double distilled water and the remaining half was dried in an oven overnight at 40 °C and then ground to powder with a mortar and pestle. The phytochemicals present in the fruit peel extract act as a capping agent and reducing agent for the synthesis of zinc oxide nanoparticles. A schematic diagram for the synthesis of NPs (P3) using peel extract is shown in Fig. 1.

### Characterization of green synthesized ZnO NPs

Absorption spectra of as-prepared NPs (P3) was measured using an advanced UV–Visible spectrophotometer (Spectramax M2<sup>o</sup>) and surface-attached functional groups were determined by Fourier transform infrared (FTIR) spectroscopy. The crystal structure of the as-synthesized NPs was determined from the powder X-ray diffraction (PXRD) pattern obtained by the D8 Discover diffractometer ( $\lambda = 0.1540$  nm,  $2\theta = 10^\circ\text{--}80^\circ$  with a scan rate  $0.02^\circ$  per second). A fluorescence emission spectrum was measured by a Carey eclipse instrument (Cary WinFLR software). Morphology of as-prepared NPs was observed using a field emission scanning electron microscope (FE-SEM, JSM-7600F, JEOL Inc, Japan) while the elemental composition was determined via in-built energy dispersive X-ray spectroscopy (EDS) of a scanning electron microscope (SEM, JSM-6610LV, JEOL Inc, Japan) at 20 kV accelerating voltage and 20–120 kX magnification at high vacuum. The zeta potential and hydrodynamic size of as-synthesized ZnO nanoparticles (P3) was determined via the dynamic light scattering (DLS—nanoPartica SZ-100-Z, Horiba) technique.

### Antibacterial studies

The antibacterial study of as-prepared NPs was performed against the gram-positive bacteria (i.e., *Streptococcus pneumoniae*, *Staphylococcus aureus*) and gram-negative bacteria (i.e., *Pseudomonas aeruginosa* and *Escherichia coli*) via broth dilution method (Garcia 2010). A stock solution (2 mg/mL) was prepared by dispersing as-prepared ZnO NPs in pre-sterilized deionized water and then diluted solutions of 0.2–200  $\mu\text{g/mL}$  were added to test tubes containing different amounts of sterile Luria Bertani broth (Muniyan et al. 2017). Next 0.5 mL of overnight culture (0.5 McFarland turbidity standards) of the target microbes was added to these tubes aseptically and incubated at 37 °C for 24 h. The bacterial cultures without any NPs suspension and the tubes with only sterile media were retained as positive and negative

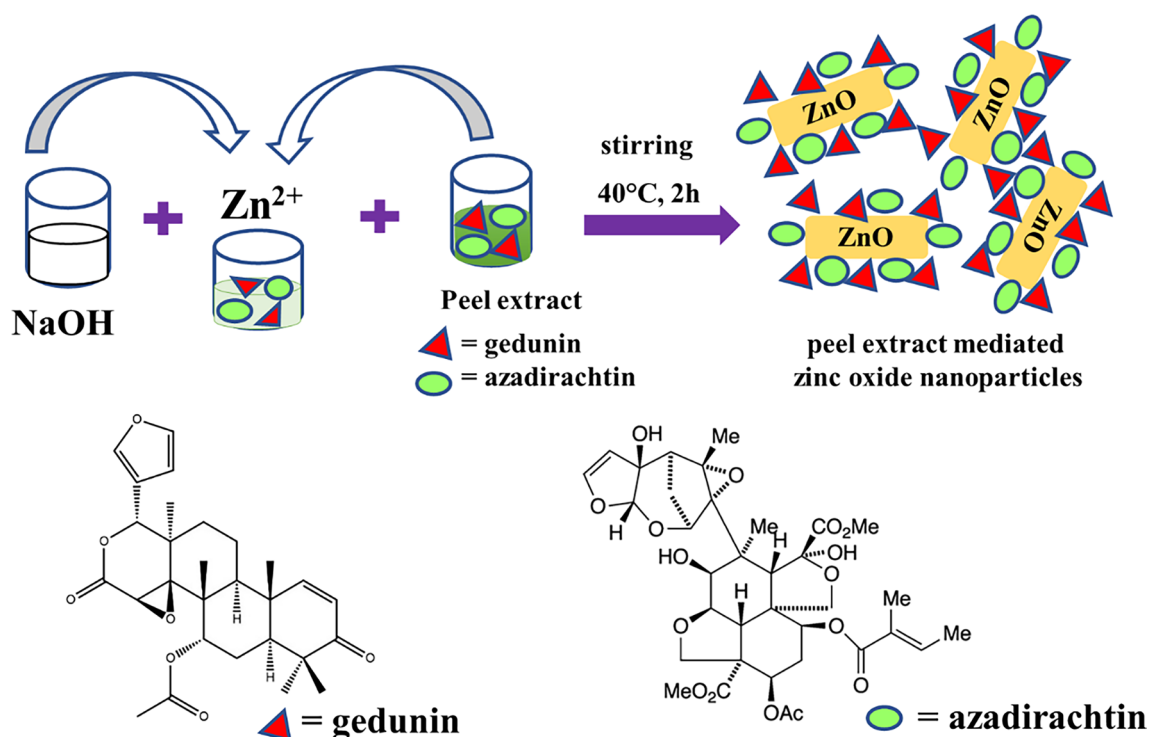


**Fig. 1** Schematic diagram representing the synthesis of zinc oxide nanoparticles (P3) using fruit peel extract of *Azadirachta indica*

controls, respectively. Antibacterial activity was determined by recording the optical density of the inoculated broth at the wavelength of 600 nm. MIC values were recorded as the lowest concentration of the test sample inhibiting the growth of the inoculated target microbes.

### Electrochemical studies

Cyclic voltammetry (CV) study of as-synthesized NPs was performed using an Electrochemical workstation (Model K-Lyte 1.2) at different scan rates of 5, 10, 20, 30, 40, and 50 mV/s. We have used 2 M KOH as an electrolyte and a three-electrode system including a modified Pt electrode (Pt electrode with drop casted synthesized ZnO NPs), standard calomel electrode, and Pt electrode as working, reference, and counter electrodes, respectively, for the electrochemical measurements. For the modification of the Pt electrode with ZnO NPs, 0.1 g of ZnO NPs was added to 1 mL of water, followed by the addition of a drop of 5% nafion solution as a binder. Then this mixture was sonicated using the digital ultrasonic cleaner (Khera, M/s Khera Instruments PVT. LTD., Model No. KI-108, India) for 30 min at 40 °C. After sonication, 3  $\mu$ L of the mixture was drop casted (drop casted using Finn timer) on Pt electrode and let dry at room temperature to get the modified Nafion/ZnO/Pt electrode. A

schematic diagram of the modified Nafion/ZnO/Pt electrode is given in Fig. 2.

### Photocatalytic studies

Photocatalytic degradation activity of as-prepared ZnO NPs is evaluated using 50 mL (10 ppm) of MB and RhB separately under sunlight irradiation. All the experiments were performed between June 30, 2022, and July 5, 2022, at Miranda House, University of Delhi, Delhi, India. All the reaction solutions were stirred for 30 min under dark conditions to achieve the adsorption–desorption equilibrium. First experiment was performed by irradiating both organic dye solutions under sunlight for 30 min without any photocatalyst. And, the second experiment was performed by irradiating both organic dye solutions under sunlight with 50 mg ZnO NPs (P3) photocatalyst in each dye solution (1 mg/mL). In the second experiment, 2 mL samples of dyes were collected at regular intervals up to 240 min of sunlight exposure. The UV–visible absorption spectroscopy (Spectramax M2<sup>e</sup> UV–visible spectrophotometer) was used to analyze these dye samples.

**Fig. 2** Schematic diagram of modified Nafion/ZnO/Pt electrode

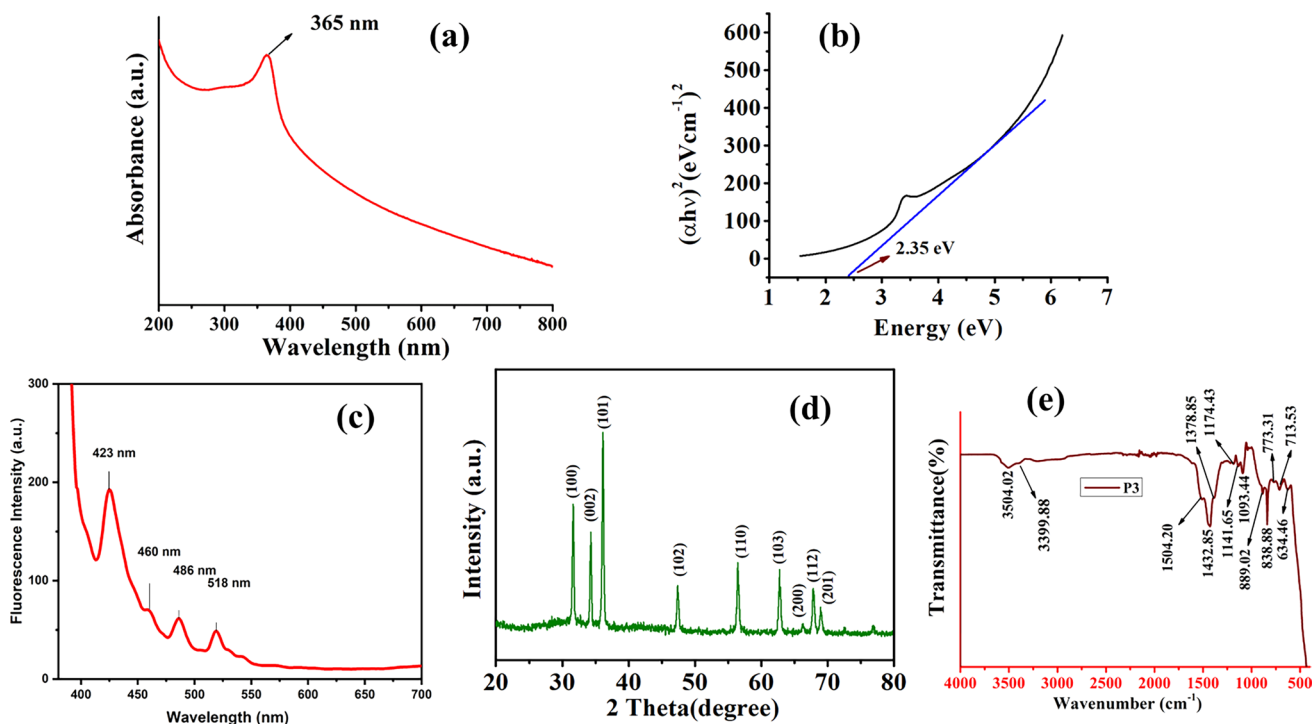
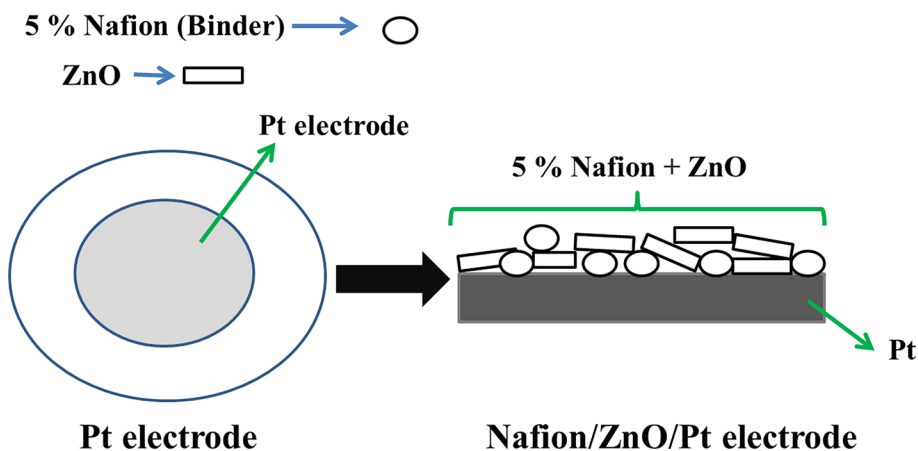


**Fig. 3** **a** UV–Visible absorption spectrum of green synthesized ZnO NPs and **b** Tauc’ plot  $(\alpha h\nu)^2$  versus  $h\nu$  (eV) of green synthesized ZnO NPs

## Results and discussions

### UV–visible spectroscopy

Figure 3a depicts the UV–Visible spectrum of as-prepared ZnO NPs. UV–Visible spectrum is recorded from 200 to 800 nm and the maximum absorption band ( $\lambda_{\max}$  (nm)) is observed at 365 nm. The strong absorbance peak obtained at 365 nm is due to surface plasmon resonance. A similar absorbance peak value was reported by Vinayagam et al. for the ZnO nanoparticles (Vinayagam et al. 2022). A relatively similar value of  $\lambda_{\max}$  is reported by other research

groups for the plant extract-mediated green synthesized ZnO NPs (Madan et al. 2016; Khara et al. 2018; Jayaseelan et al. 2012; Padalia and Chanda 2017; Vijayakumar et al. 2015). The tauc plot is drawn using the UV–Visible absorption spectrum data by applying the following tauc equation (Eq. 1). The value of  $\gamma$  is found to be  $\frac{1}{2}$  for the direct and 2 for the indirect band, respectively.

$$(\alpha h\nu)^{\frac{1}{\gamma}} = A(h\nu - E_g) \tag{1}$$

where  $\alpha$  is the energy-dependent absorption coefficient,  $h$  is the Planck constant,  $\nu$  is the photon’s frequency,  $E_g$  is the band gap energy, and  $A$  is a constant.

The energy band gap ( $E_g = 2.35$  eV) is determined from the intercept of  $(ah\nu)^2$  versus  $h\nu$  curve as shown in Fig. 3b. Similar,  $E_g$  value is reported for *Azadirachta indica* leaf extract-mediated green synthesized ZnO NPs (Rani et al. 2022a, b, c).

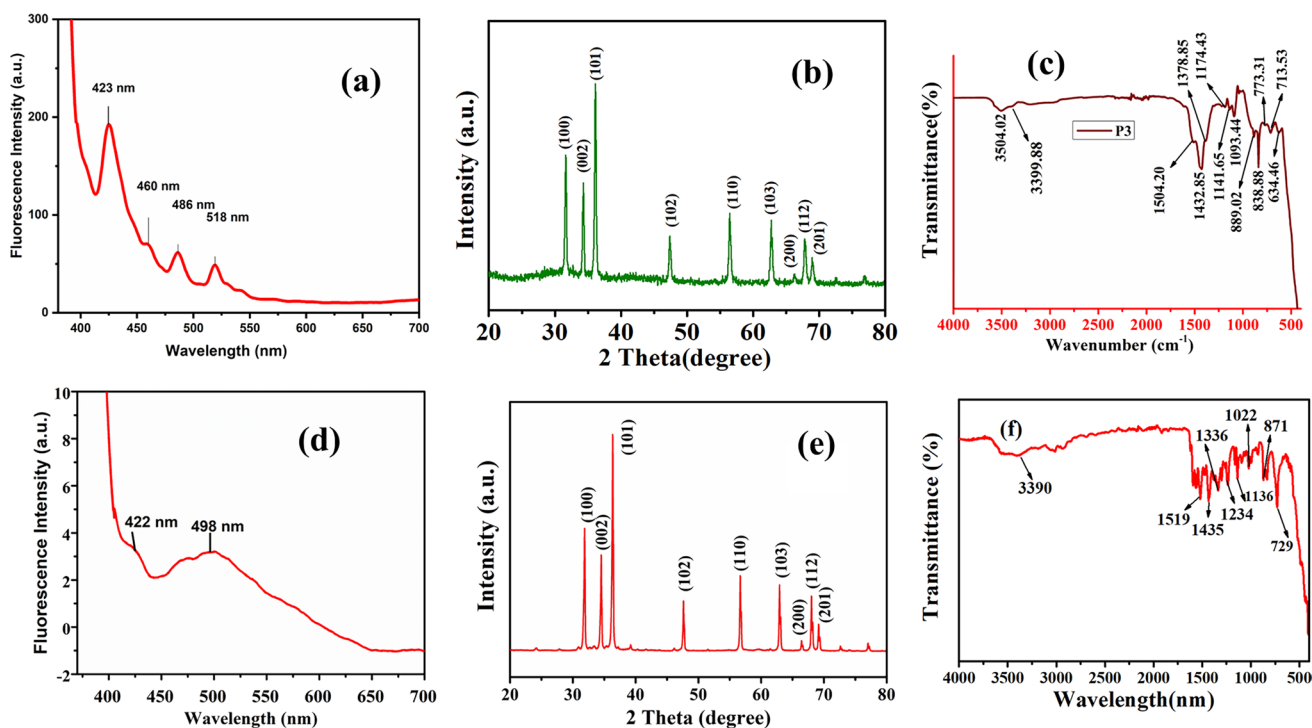
## Fluorescence spectroscopy

Figure 4a shows the fluorescence emission spectrum of as-synthesized ZnO NPs in the range from 382 to 700 nm at an excitation wavelength of 372 nm. The characteristics peaks were observed at 423, 460, 486, and 518 nm confirming the formation of pure ZnO nanoparticles. The peak at 423 nm originated due to the formation of interstitial defects in Zn while the peak at 460 nm and 486 nm emerged due to the creation of oxygen vacancy defects. Further, the visible luminescence peak at 518 nm (attributed to antisite defect) associated with deep-level or trap state emission which is originated due to the transition from the deep donor level (by oxygen vacancies in ZnO) to the valence band. Similar emission peaks are reported for ZnO nanoparticles synthesized via different approaches (Irimpan et al. 2007; Djurišić et al. 2004). For example, Madan et al. reported the emission peak at 501 nm at an excitation wavelength of 376 nm (Madan et al. 2016).

Figure 4d depicts the emission spectra of commercialized ZnO powder. The fluorescence spectrum has been recorded using Carey eclipse instrument (Model No. G9800AA) from 382 to 700 nm at an excitation wavelength of 372 nm. The emission spectrum of commercial ZnO NPs (Fig. 4d) shows peaks at 422 nm and 498 nm corresponds to the characteristics emission of due to its wide band gap and formation of vacancy defects, respectively. There is no sharp peak found in the region from 450 to 550 nm. Whereas, there are sharp peaks at 460, 486, and 518 nm in the green synthesized ZnO NPs. On comparing the emission spectra of green synthesized ZnO NPs with the commercialized one, we have found that the intensity of visible emission increases in the green synthesized ZnO NPs.

## Powder X-ray diffraction

Figure 4b shows the PXRD pattern of as-prepared ZnO NPs. The peaks are observed at  $2\theta = 31.72^\circ$ ,  $34.42^\circ$ ,  $36.20^\circ$ ,  $47.42^\circ$ ,  $56.48^\circ$ ,  $62.58^\circ$ ,  $66.26^\circ$ ,  $67.70^\circ$ ,  $68.80^\circ$ ,  $72.42^\circ$  and  $76.70^\circ$  corresponding to the (hkl) planes (100), (002), (101), (102), (110), (103), (200), (112), (201), (004) and (202), respectively. The obtained intensity of peaks and their corresponding (hkl) values show the hexagonal wurtzite crystalline structure of ZnO NPs. These  $2\theta$  values have been matched with the reported JCPDS No. 36-1451 (Ji et al.



**Fig. 4** **a** Emission spectrum of green synthesized ZnO NPs, **b** Powder X-ray Diffraction Pattern for green synthesized ZnO NPs, **c** FTIR spectrum of green synthesized ZnO NPs, **d** Emission spectrum of

commercialized ZnO NPs, **e** Powder X-ray Diffraction Pattern for commercialized ZnO NPs, **f** FTIR spectrum of commercialized ZnO NPs

2016). Figure 4e displays the PXRD pattern of commercial ZnO NPs. The peak positions ( $2\theta$  values) of commercialized ZnO NPs are obtained same as-synthesized ZnO NPs (P3). However, peak intensities for commercial ZnO NPs have been investigated higher than the green synthesized ZnO NPs (P3). The crystallite size of the commercial ZnO has been calculated using the Scherrer equation (Eq. 2).

$$D = \frac{k\lambda}{\beta \cos \theta} \quad (2)$$

where  $D$  is the crystallite size of synthesized material,  $\lambda$  is the X-ray wavelength (0.154 nm),  $k$  is the Scherrer constant (0.9),  $\beta$  is the full width at the half maximum intensity of diffraction peak (FWHM), and  $\theta$  is the Bragg angle of diffraction peak. The calculated average crystallite size of commercial ZnO is 33.972 nm. Whereas the size of the crystallite of green synthesized ZnO NPs (P3) has been found less than the commercial ZnO NPs.

### Fourier transform infrared (FTIR) spectroscopy

Figure 4c shows the FTIR spectra of as-prepared ZnO NPs recorded in the range of 500–4000  $\text{cm}^{-1}$ . Herein, bands at 634.46–773.31  $\text{cm}^{-1}$  are due to  $-\text{Zn}-\text{O}-$  stretching vibration

of ZnO NPs, and bands between 773.31 and 3504.02  $\text{cm}^{-1}$  are correlated to the functional groups of surface-attached phytochemicals coating of biosynthesized ZnO NPs. These functional groups are observed because of the phytochemicals that are present in the extract of *Azadirachta indica* fruit peels as derivatives of phenol (Thymol), monoterpene, trans-hydrate Sabineno, polyphenolic acids, and flavonoids. Azadirachtin, an important tetranortriterpenoid is a commercialized biopesticide (Kilani-Morakchi et al. 2021). The bands at 838.88–889.02  $\text{cm}^{-1}$  are associated with the stretching vibration of carbonate species while bands at 1093.44, 1141.65, 1174.43, and 1378.85  $\text{cm}^{-1}$  are related to the aromatic  $-\text{C}-\text{H}$  bond. In addition, bands at 1432.85–1504.20  $\text{cm}^{-1}$  and 3399.88–3504.02  $\text{cm}^{-1}$  are due to  $-\text{C}-\text{O}$  bond and  $\text{H}_2\text{O}$  or  $-\text{O}-\text{H}$  stretching vibration, respectively. Our FTIR analysis is in good agreement with reported FTIR data for green synthesized ZnO NPs (Umar et al. 2009; Ramesh et al. 2015; Basri et al. 2020). Figure 4(f) depicts the FTIR spectra of commercial ZnO NPs recorded in the range of 500–4000  $\text{cm}^{-1}$ . It is clear from this FTIR spectrum that there is little difference in the corresponding vibration band positions as well as their intensities of commercial ZnO NPs and as-synthesized ZnO NPs. This difference is found because of the use of different precursors (stabilizing/capping & reducing agents) in their synthesis.

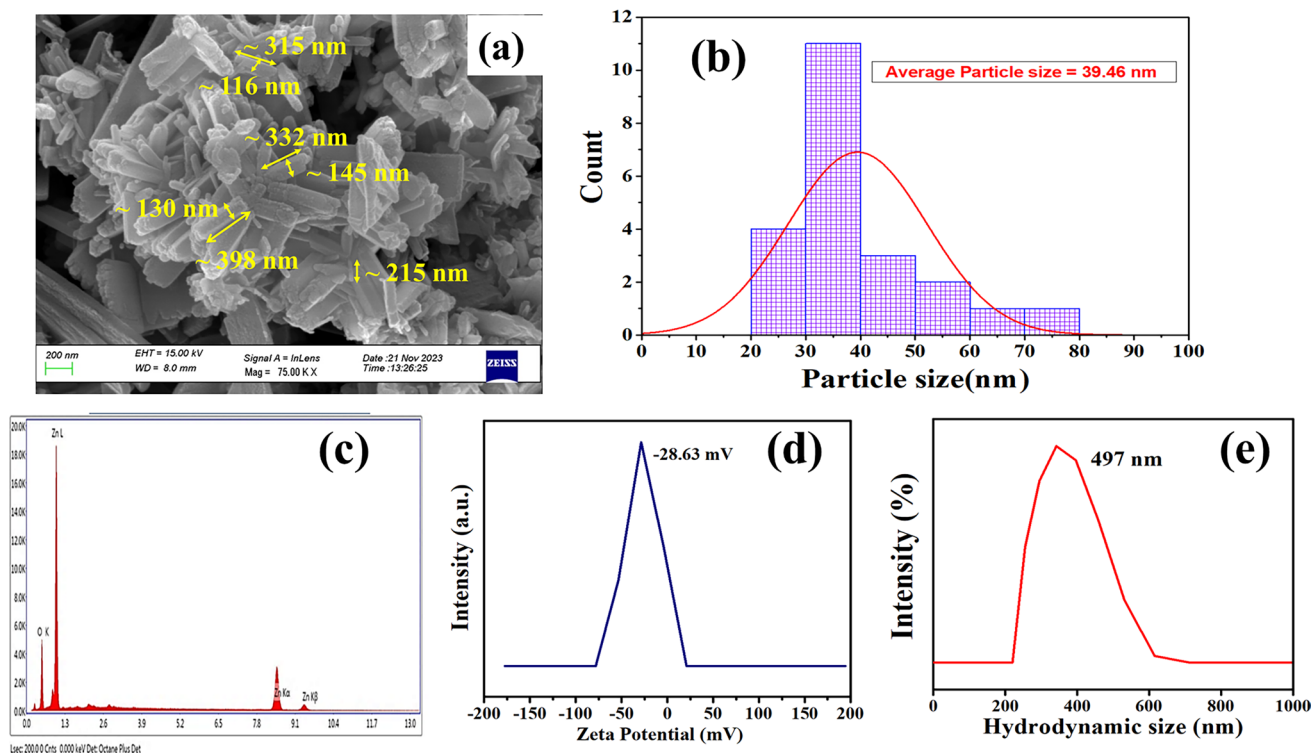


**Fig. 5** a FE-SEM image of green synthesized ZnO nanoparticles (at 15.0 kV, at 75.00 kx magnification), b histogram showing the average particle size of ZnO (P3) nanoparticles and c EDS spectrum of green

fabricated ZnO nanoparticles d zeta potential plot of green synthesized ZnO (P3) nanoparticles e hydrodynamic size of the green synthesized ZnO (P3) nanoparticles

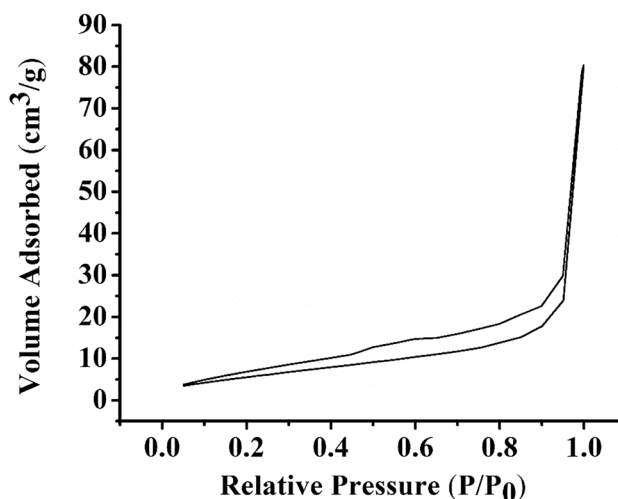
## FE-SEM/EDS and DLS

Figure 5a depicts the FE-SEM image of as-synthesized ZnO NPs which are found to be flake-shaped with 116–145 nm width and 215–398 nm length. It can be seen that as-prepared ZnO NPs are flake-shaped (micro to nano-sized) and agglomerated due to interlinking surface-attached functional groups of phytochemicals (as confirmed by FTIR) which played a key role to control the morphology of green synthesized NPs. Our FE-SEM results are relatively similar to the reported biosynthesized 73–123 nm ZnO NPs by Basri et al. (2020). The histogram shown in Fig. 5b depicted the average particle size of the synthesized ZnO NPs. The average size is found to be 39.46 nm using ImageJ software. Figure 5c shows the EDS analysis of green synthesized ZnO NPs and the corresponding elemental composition is given in Table 1. The atomic percentage of zinc (Zn) and oxygen (O) atoms are determined as 43.2% and 56.8%, respectively. The higher atomic % of oxygen (O) atoms could lead to the formation of unstable ZnO<sub>2</sub> nanoparticles. Jannesari et al. (2023) also demonstrated the formation of reduced graphene oxide (rGO)/ZnO<sub>2</sub>-Ag nanoframeworks and their application for antibacterial activity. The zeta potential plot of green synthesized ZnO nanoparticles (P3) dispersed in an aqueous suspension is shown in Fig. 5d. The zeta potential value of -28.63 mV confirms colloidal stability as similar to the reported zeta potential value of -28 mV for ZnO nanoparticles/carbon nanodots hybrid composites (Hamed et al. 2023). Figure 5e indicated the DLS plot for the hydrodynamic size ( $D_h$ ) of the green synthesized ZnO (P3) nanoparticles suspended in an aqueous media. It can be seen that  $D_h$  of the as-prepared ZnO NPs (497 nm) is relatively larger than their corresponding FE-SEM size. This could be due to (1) the presence of a hydration layer around the ZnO NPs via interactions between the functional groups of the surface-attached phytochemical coating molecules (as confirmed by FTIR) and surrounding water molecules (2) the formation of small aggregates of flake-shaped ZnO NPs in their aqueous suspension (Maity and Agrawal 2007; Kandasamy et al. 2019).

**Table 1** Energy dispersive spectroscopy (EDS) analysis of green synthesized ZnO NPs

Element	Weight %	Atomic %	Net Int.	Error %
O K	24.34	56.8	143.03	8.35
Zn K	75.66	43.2	244.47	2.35

\*Weight % = weight percentage, Atomic % = atomic percentage, Net Int. = Net intensity



**Fig. 6** N<sub>2</sub> adsorption/desorption isotherms of synthesized ZnO NPs (P3)

## Brunauer–Emmett–Teller (BET) of synthesized ZnO nanoparticles (P3)

The N<sub>2</sub> adsorption/desorption (BET) isotherm of the ZnO NPs (P3) is shown in Fig. 6. According to IUPAC, the synthesized ZnO NPs (P3) exhibit a type IV adsorption/desorption isotherm (Liang et al. 2015). The synthesized ZnO NPs (P3) show an adsorption/desorption hysteresis loop of type H3. The H3 adsorption/desorption hysteresis loop reveals that synthesized ZnO NPs (P3) are mesoporous (Yadav et al. 2023a, b, c). The synthesized ZnO NPs (P3) have a surface area of 22.721 m<sup>2</sup>/g. Whereas the surface area have been calculated as 14.234 m<sup>2</sup>/g for B3 and 18.738 m<sup>2</sup>/g for the S3 sample.

## Antibacterial activities

Antibacterial activity of as-prepared ZnO NPs (P3) is performed on *Escherichia coli*, *Pseudomonas aeruginosa*, *Staphylococcus aureus*, and *Streptococcus pneumoniae* using broth dilution method and corresponding minimum inhibitory concentration (MIC) values are given in Table 2.

**Table 2** Minimum Inhibitory Concentration (MIC) of biosynthesized ZnO nanoparticles (P3) for various bacterial pathogens

Isolates	MIC value (μg/mL)
<i>Escherichia coli</i>	135
<i>Pseudomonas aeruginosa</i>	140
<i>Staphylococcus aureus</i>	130
<i>Streptococcus pneumoniae</i>	130



The MIC values are determined as 140 µg/mL for *Pseudomonas aeruginosa*, 135 µg/mL for *Escherichia coli*, and 130 µg/mL for both *Staphylococcus aureus* and *Streptococcus pneumoniae*. Higher MIC values for gram-negative bacteria (*Escherichia coli* and *Pseudomonas aeruginosa*) indicate that these microbes are more resistant than gram-negative bacteria (*Staphylococcus aureus* and *Streptococcus pneumoniae*). In other words, a higher concentration of as-synthesized ZnO NPs is required to kill the gram-negative bacteria than the gram-positive bacteria. Thus green synthesized ZnO NPs are more effective against gram-positive bacteria than gram-negative bacteria. Our results are in good agreement with the reported antimicrobial activity of green synthesized ZnO NPs with concentrations of 25–100 µg/mL (Sana et al. 2020). Similar antibacterial study has also been performed with green synthesized ZnO nanoparticles with leaf extract of *Azadirachta indica* (Elumalai and Velmurugan 2015). Herein, the concentration of ZnO nanoparticles varies in the range of 50–100 µg/mL. In this study, the antibacterial activities increases because of increase in the concentration of H<sub>2</sub>O<sub>2</sub> from the surface of ZnO nanoparticles. In our earlier work, we synthesized ZnO nanoparticles (S3 and F1) using seed extract and fruit extract of *Azadirachta indica*, respectively, to study their antibacterial activity (Saini et al. 2022a,

b, c). As compared to S3 and F1, P3 exhibits better antibacterial performance against *Pseudomonas aeruginosa*, whereas against *Escherichia coli* it shows similar antibacterial activity to S3 (refer Table S1). Furthermore, compared to F1, the antibacterial activity exhibited by P3 was more against *Staphylococcus aureus*. Table 3 represents a comparison of MIC values of as-synthesized ZnO NPs with reported ZnO-based nanostructured materials which are synthesized using different plant extracts and evaluated for their antibacterial activities against various bacterial pathogens (Arvanag et al. 2019; Elumalai et al. 2015; Fouladi-Fard et al. 2022; Imade et al. 2022; Subramanian et al. 2022; Velsankar et al. 2022; Alotaibi et al. 2022). Akhavan et al. (2009) reported that hydrothermally synthesized ZnO nanorod array exhibited good photocatalytic degradation of *E. coli* bacteria.

Several reports on antibacterial mechanisms explained the mechanistic pathways for antibacterial activity. For example, Akhavan and Ghaderi (Akhavan and Ghaderi 2010) reported the antibacterial effect was due to the direct interaction of the nanowalls of graphene oxide with the cell membrane of the bacteria used in this study. The sharper edges of the reduced graphene oxide nanowalls permitted more contact interaction with the cell membrane of the bacteria and resulted in higher toxicity.

**Table 3** A comparison of reported ZnO-based nanostructured materials with as-synthesized ZnO nanoparticles for antibacterial activities

S. no.	Nanoparticles	Plant extract used for biosynthesis	Organism/MIC value	References
1	ZnO	<i>Murraya koenigii</i>	<i>Staphylococcus aureus</i> /25 µg/mL <i>Escherichia coli</i> /50 µg/mL <i>Bacillus subtilis</i> /100 µg/mL	Elumalai et al. (2015)
2	ZnO	<i>Azadirachta indica</i>	<i>Staphylococcus aureus</i> /6.25 µg/mL <i>Escherichia coli</i> /25 µg/mL <i>Bacillus subtilis</i> /6.25 µg/mL	Elumalai et al. (2015)
3	Ag/ZnO	<i>Crataegus monogyna</i>	<i>Staphylococcus aureus</i> /200 µg/mL <i>Pseudomonas aeruginosa</i> /200 µg/mL <i>Klebsiella pneumoniae</i> /50 µg/mL	Fouladi-Fard et al. (2022)
4	ZnO	<i>Musa paradisiaca</i>	<i>Bacillus cereus</i> /100 µg/mL <i>Staphylococcus aureus</i> /100 µg/mL <i>Klebsiella pneumoniae</i> /100 µg/mL <i>Salmonella enterica</i> /100 µg/mL	Imade et al. (2022)
5	ZnO	<i>Sargassum muticum</i>	<i>Acinetobacter baumannii</i> /200 µg/mL <i>Pseudomonas stutzeri</i> /200 µg/mL <i>Bacillus flexus</i> /200 µg/mL	Subramanian et al. (2022)
6	ZnO	<i>Erythrina variegata</i>	<i>Staphylococcus aureus</i> /150 µg/mL <i>Bacillus subtilis</i> /150 µg/mL <i>Salmonella typhi</i> /150 µg/mL	Velsankar et al. (2022)
7	ZnO	<i>Gardenia thailandica</i>	<i>Pseudomonas aeruginosa</i> /64 µg/mL	Alotaibi et al. (2022)
8	ZnO	<i>Origanum majorana</i>	<i>Pseudomonas aeruginosa</i> /175 µg/mL <i>Escherichia coli</i> /125 µg/mL <i>Staphylococcus aureus</i> /100 µg/mL <i>Streptococcus pneumoniae</i> /100 µg/mL	Saini et al. (2022a, b, c)
9	ZnO	<i>Azadirachta indica</i>	<i>Klebsiella aerogenes</i> /150 µg/mL <i>Staphylococcus aureus</i> /200 µg/mL	Madan et al. (2016)
10	ZnO	<i>Silybum marianum</i> L	<i>Escherichia coli</i> /0.4 mg/mL	Arvanag et al. (2019)
11	ZnO	<i>Azadirachta indica</i>	<i>Pseudomonas aeruginosa</i> /140 µg/mL <i>Escherichia coli</i> /135 µg/mL <i>Streptococcus Pneumoniae</i> /130 µg/mL <i>Staphylococcus aureus</i> /130 µg/mL	Present work

On the other hand, Prasanna and Vijayaraghavan (2015) reported that the antibacterial activity shown by ZnO nanoparticles was due to ROS generation even in the dark. It is also reported that aggregated graphene nanosheets may capture and inactivate *Escherichia coli* bacteria by encapsulating them (Akhavan et al. 2011). Likewise, Liu et al. (2011) reported that the mechanism involved in the antibacterial activity exhibited by graphene oxide was due to both oxidative stress and membrane disruption of the bacteria. Similarly, oxidative stress and DNA damage were caused for the antibacterial activity demonstrated by ZnO and TiO<sub>2</sub> nanoparticles (Kumar et al. 2011). In another study, Wang et al. studied the antibacterial activity of the ZnO/GO nanocomposites. Initially, the ZnO/GO nanocomposites wrapped the bacteria and caused bacterial damage by increasing the localized zinc concentration (Wang et al. 2014). Jannesari et al. (2020) recently reported that the generation of O<sub>2</sub> nanobubbles from graphene/CuO<sub>2</sub> nanocomposites was responsible for disrupting the bacterial respiration process. Methanolic extracts of *Azadirachta indica* (Neem) fruit mesocarp and epicarp have shown antibacterial activity against the human pathogenic and plant pathogenic isolates *Acinetobacter johnsonii* (gram-positive), *Agrobacterium tumefaciens*, respectively (Ibrahim et al 2022). This study was also done with *Serratia marcescens* (gram-negative) bacteria. Growth inhibition of these bacteria has been reported at the concentration of 62.5 µg/mL for both extracts, Herein, the growth inhibition increases significantly as the extract concentration increases. The maximum inhibition in growth of these bacteria has been obtained at the highest concentration (1000 µg/mL). It is reported that fruit epicarp extract displays more antimicrobial activity against these three bacteria as compared to fruit mesocarp extract. A comparative study has been performed with the amoxicillin antibiotics. In this study, the extract of epicarp and mesocarp show the highest antimicrobial activity against the *Acinetobacter johnsonii*. The percentage growth inhibition of all tested bacteria has been found more with fruit (peel: epicarp) extract than with the amoxicillin antibiotic. Figure 7 depicts the plausible schematic mechanism for the antibacterial activity demonstrated by metal oxide nanoparticles. According to the literature survey, different kinds of mechanisms are utilized by metal oxide nanoparticles that function as antibacterial agents. In our previously published paper, we reported the antibacterial activity of the ZnO nanoparticles was due to the disruption of the bacterial cell membrane/wall. These ZnO nanoparticles were synthesized using leave extract of *Nyctanthes arbor-tristis* plant (Rani et al. 2023). In the present research paper, one type of bacteria (*Staphylococcus aureus*) out of the studied bacteria and the composition of synthesized metal oxide NPs (ZnO: P3) are the same, only the extract used in this

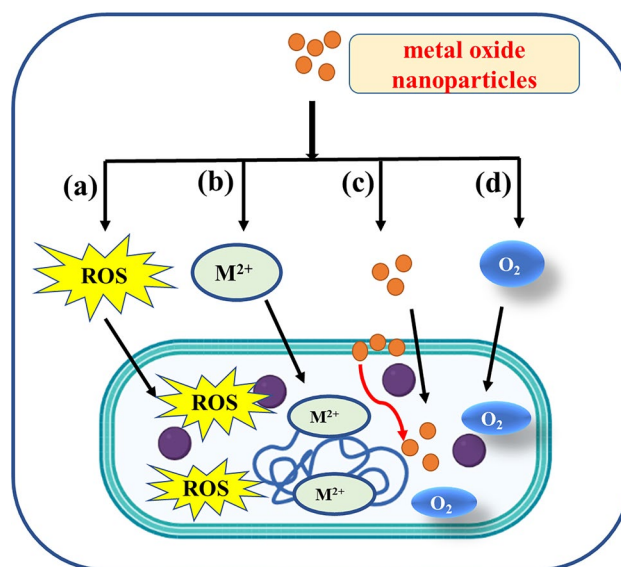


**Fig. 7** Schematic plausible mechanism for antibacterial activity exhibited by metal oxide nanoparticles **a** reactive oxygen species (ROS) generation (Prasanna and Vijayaraghavan 2015) **b** formation of M<sup>2+</sup> (Wang et al. 2014) **c** attachment of metal oxide nanoparticles onto the surface of bacteria (Rani et al. 2023) **d** formation of O<sub>2</sub> nanobubbles (Jannesari et al. 2020)

synthesis is different. So the same mechanism, i.e., interaction of ZnO (P3) nanoparticles with the bacterial cells might be taking place (disruption of cell membrane/wall).

### Electrochemical activities

The cyclic voltammetry technique is used to determine the electrochemical activity in the presence of 2 M KOH electrolyte to evaluate the performance of green synthesized NPs (P3) for supercapacitor application. Figure 8a shows the cyclic voltammograms (i.e., CV curves) of as-synthesized ZnO NPs electrode at different scan rates (5–50 mV/s) and Fig. 8b presents the specific capacitance vs scan rates graph. Specific capacitance ( $C_s$ ) and energy density ( $E$ ) are estimated using Eqs. (3) and (4) as mentioned below (Yadav et al. 2022a, b).

$$C_s = \frac{\int I}{mS(V_2 - V_1)} \quad (3)$$

$$E = \frac{1}{2} \frac{1000}{3600} (C_s)(V)^2 \quad (4)$$

where  $I$  (A) is the integrated current area,  $m$  (g) is the mass of the electrode material,  $(V_2 - V_1)$  and  $V$  (V) is the potential window,  $S$  (mV/s) is the scan rate,  $C_s$  (F/g) is the specific capacitance and  $E$  (Wh/kg) is the energy density.

**Fig. 8** **a** Cyclic voltammograms and **b** specific capacitance versus scan rate plot for as-synthesized ZnO NPs

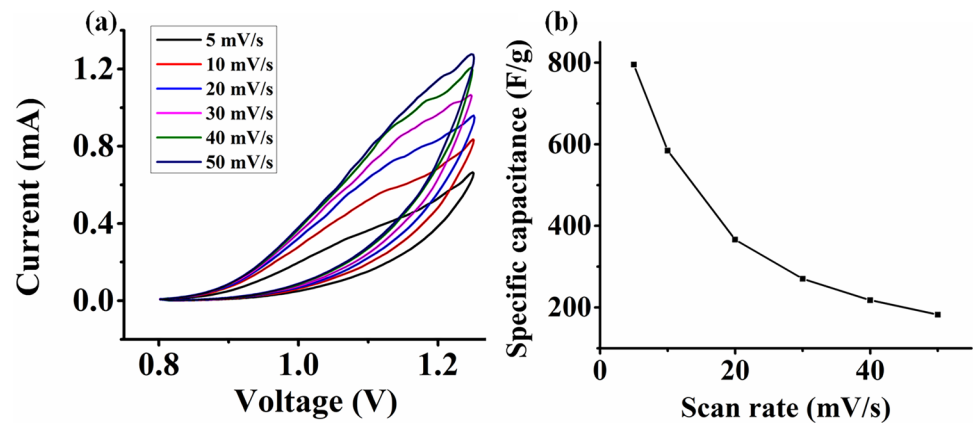


**Table 4** Estimated specific capacitance and energy density values of as-synthesized ZnO NPs at different scan rates

s. no.	Scan rate (mV/s)	Specific capacitance (F/g)	Energy density (Wh/kg)
1	5	794.96	22.3392
2	10	584.28	16.4185
3	20	366.43	10.2968
4	30	270.34	7.5967
5	40	218.03	6.1267
6	50	182.53	5.1291

The calculated specific capacitance and energy density values of biosynthesized ZnO NPs at different scan rates are given in Table 4. The highest specific capacitance value of 794.96 F/g and energy density value of 22.3392 Wh/Kg are observed at the lowest scan rate, i.e., 5 mV/s. Moreover, the specific capacitance value gradually decreases with the increment of the scan rate from 5 to 50 mV/s (refer to Fig. 6b). Thus, it reveals that an as-synthesized ZnO nanoparticles electrode has high storage efficiency at a lower scan

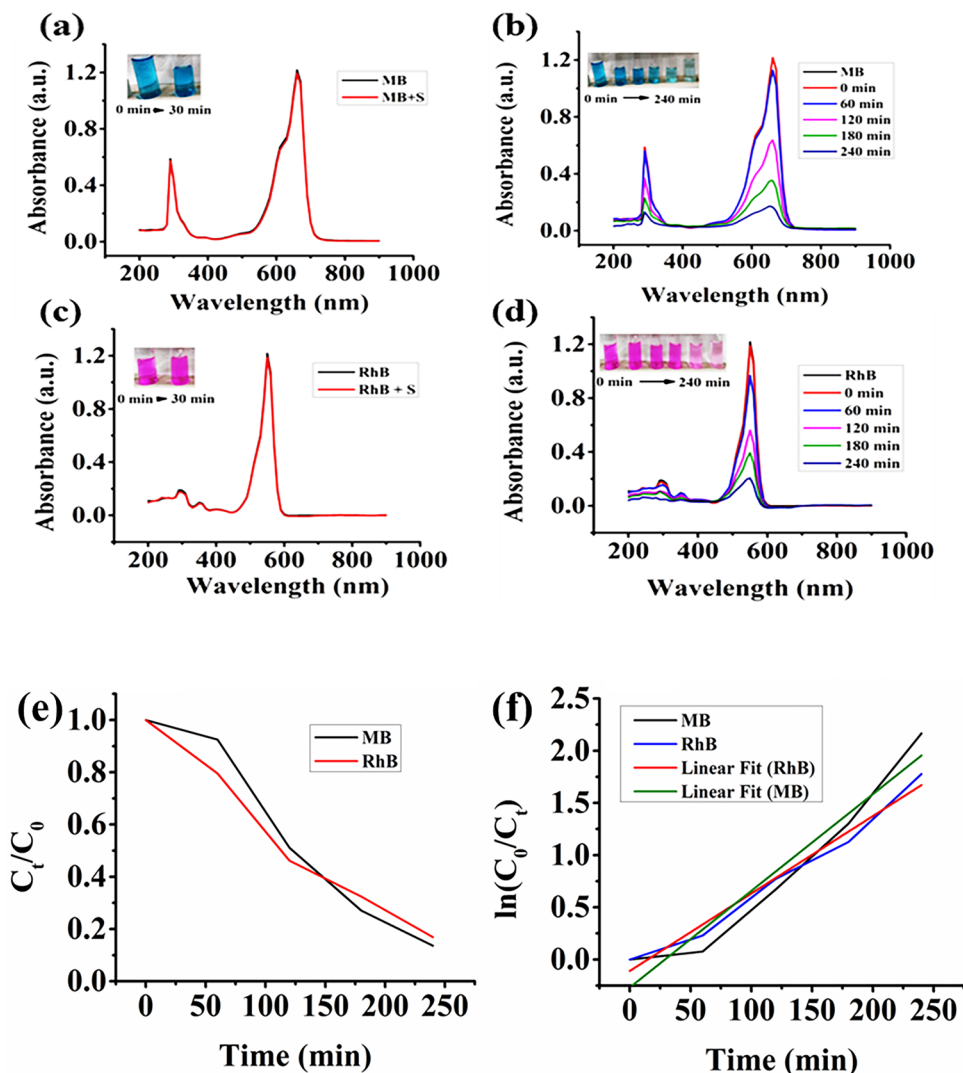
rate. A similar trend was reported with Ni-doped ZnO nanostructure (Mohan et al. 2022). In our previously reported work, ZnO nanoparticles (S3 and B3—synthesized using seed and bark extract of *Azadirachta indica*) have shown specific capacitance of 1.53 F/g and 1.27 F/g, respectively, at the scan rate of 20 mV/s (Saini et al. 2022a, b, c). Hence, as-prepared ZnO NPs (P3—synthesized using fruit peel extract of *Azadirachta indica*) showed higher specific capacitance value (366.43 F/g) than previously reported specific capacitance value for S3 and B3 at the same scan rate of 20 mV/s (refer Table S1). Because of the higher surface area (22.721 m<sup>2</sup>/g), the green synthesized ZnO nanoparticles (P3) show a higher value of specific capacitance than the synthesized ZnO nanoparticles (B3:14.234 m<sup>2</sup>/g; S3: 18.738 m<sup>2</sup>/g).

The plausible reason for this enhanced specific capacitance of as-synthesized ZnO NPs electrode is its high surface-to-volume ratio. The specific capacitance value of ZnO NPs can be further enhanced by doping of metal/metal oxides, carbon-based nanomaterials, conducting polymers, etc. (Yadav et al. 2022a, b). Nethaji et al. reported an enhanced specific capacitance of the V<sub>0.07</sub>Ag<sub>0.07</sub>ZnO electrode (2700.19 F/g) than the ZnO electrode (402.1 F/g)

**Table 5** A comparison of as-synthesized ZnO NPs with previously reported ZnO based nanostructured materials-based electrodes for supercapacitor applications

S. no.	Electrode material	Synthesis method	Specific capacitance (F/g)	Scan rate (mV/s)	References
1	Ni-doped ZnO nanoparticles	Chemical co-precipitation method	133	10	Mohan et al. (2022)
2	V <sub>0.07</sub> Ag <sub>0.07</sub> ZnO nanocomposites	One-step sol–gel method	2700.19	5	Nethaji and Kumar (2022)
3	ZnO nanoparticles	One-step sol–gel method	402.1	5	Nethaji and Kumar (2022)
4	ZnO nanoparticles	Biosynthesis method	6.32	20	Yadav et al. (2022a)
5	CeO <sub>2</sub> –ZnO nanocomposite	Biosynthesis method	431	5	Choubari et al. (2022)
6	ZnO/CNT/Fe <sub>3</sub> O <sub>4</sub> /Ni foam nanocomposites	Chemical vapor deposition and hydrothermal method	532	10	Moghadam and Seif (2022)
7	ZnO nanoparticles	Biosynthesis method	535.71	20	Rani et al. (2020)
8	ZnO nanoparticles	Biosynthesis method	794.96	5	This work

**Fig. 9** **a** UV–visible spectrum of MB dye after 30 min exposure to sunlight in the absence of ZnO NPs, **b** UV–visible spectra of MB dye after exposure to sunlight at different time intervals in the presence of as-synthesized ZnO NPs, **c** UV–visible spectrum of RhB dye after 30 min exposure of sunlight in absence of ZnO NPs and **d** UV–visible spectra of RhB dye after exposure of sunlight at different time intervals in presence of as-prepared ZnO NPs. **e**  $C_t/C_0$  versus time of sunlight irradiation plot for photocatalytic degradation reactions of MB and RhB dyes in the presence of as-synthesized ZnO NPs and **f** photocatalytic degradation kinetics of MB and RhB dyes in the presence of synthesized ZnO NPs



(Nethaji and Kumar 2022). Similarly, Buldu-Akturk et al. (2022) have also reported enhanced electrochemical performance of reduced graphene oxide/zinc oxide (rGO/ZnO) hybrid nanocomposites than individual ZnO-based supercapacitor electrodes. A comparative electrochemical study of as-synthesized ZnO NPs electrode with recently reported ZnO-based nanostructured materials is given in Table 5.

### Photocatalytic activities

Figure 9 presents the UV–visible spectra of organic dyes (i.e., MB and RhB) for photocatalytic degradation (due to sunlight irradiation) in the absence or presence of as-synthesized ZnO NPs (P3). Figure 9a and c shows the UV–visible spectra for blank photocatalytic degradation reactions of MB and RhB under 30 min exposure to sunlight, respectively. There is no dye degradation in the absence of ZnO NPs under sunlight irradiation because no visible decrease in  $\lambda_{\max}$  values is observed for both the MB/RhB dyes. Figure 9b and

d depicts the UV–visible spectra for photocatalytic degradation reactions of MB and RhB under exposure to sunlight at different time intervals in the presence of ZnO synthesized NPs. It can be seen that there is a decrease in  $\lambda_{\max}$  values for both the MB/RhB dyes indicating the decrease in the concentration of dyes due to the photocatalytic degradation reaction in the presence of ZnO NPs under sunlight irradiation. The photocatalytic degradation efficiency is calculated using Eq. (5) (Yadav et al. 2022a, b).

$$\text{Efficiency \%} = \left[ \frac{(C_0 - C_t)}{C_t} \right] \times 100 \quad (5)$$

where  $C_0$  is the initial concentration of an organic dye and  $C_t$  is the concentration of a dye at different time intervals.

It is observed that 88.53% of MB dye and 83.08% of RhB dye are degraded in the presence of as-synthesized ZnO NPs (P3) after 240 min exposure to sunlight. Thus the photocatalytic degradation efficiency of the as-prepared ZnO NPs is

found to be slightly higher for the MB dye than the RhB dye under 240 min of sunlight irradiation. In our previous article (Saini et al. 2022a, b, c), we reported 84.62% degradation efficiency of methyl orange dye for ZnO nanoparticles (B3—synthesized using bark extract of *Azadirachta indica*) under 180 min of UV–visible light irradiation (refer to Table S1).

Figure 9e shows  $C_t/C_0$  versus time ( $t$ ) of sunlight irradiation plot for photocatalytic degradation reaction of both the MB/RhB dyes in the presence of synthesized ZnO NPs. It can be seen that the photocatalytic activity of as-synthesized ZnO NPs is slightly higher for RhB than MB from the beginning ( $t=0$ ) up to 150 min of sunlight exposure. However, the photocatalytic activity of as-synthesized ZnO NPs is found to be slightly higher for MB than RhB above 150 min of sunlight exposure toward the end of the degradation reaction ( $t=240$  min). Overall, as-synthesized ZnO NPs have shown relatively similar photocatalytic degradation behavior (i.e., concentration for dyes gradually decreases with sunlight exposure time) for both MB and RhB dyes. Furthermore, the kinetic studies of photocatalytic degradation of MB/RhB dyes in the presence of the as-synthesized ZnO NPs are displayed in Fig. 9f. The following pseudo-first-order kinetics Eq. (6) is used to calculate degradation rate constants for the corresponding photocatalytic dye degradation reaction

(linear fitted straight lines indicate pseudo-first-order kinetics) (Alotaibi et al. 2022).

$$\ln\left(\frac{C_0}{C_t}\right) = -kt \quad (6)$$

where  $C_0$  is the initial concentration of dye solutions,  $C_t$  is the concentration of dye solutions at time intervals  $t$ ,  $t$  is the time of sunlight exposure (min) and  $k$  is the rate constant ( $\text{min}^{-1}$ ).

The photocatalytic degradation reactions rate constant value is estimated as  $0.0092 \text{ min}^{-1}$  and  $0.0074 \text{ min}^{-1}$  for MB and RhB, respectively, and thus as-synthesized ZnO NPs showed a higher photodegradation rate for MB than RhB under sunlight irradiation.

The UV–visible spectra of methylene blue (MB) and rhodamine B (RhB) dyes during the reaction in the presence of synthesized ZnO NPs (P3) under dark conditions are given in Fig. 10a and b, respectively. It is observed that there is no visible decrease in  $\lambda_{\text{max}}$  values observed for both the organic dyes and no dye degradation is detected for both of the chosen organic dyes in the presence of synthesized ZnO NPs (P3) under dark conditions. The reusability study of synthesized ZnO nanoparticles for the degradation of MB dye and RhB dye is given in Fig. 10c. Synthesized ZnO

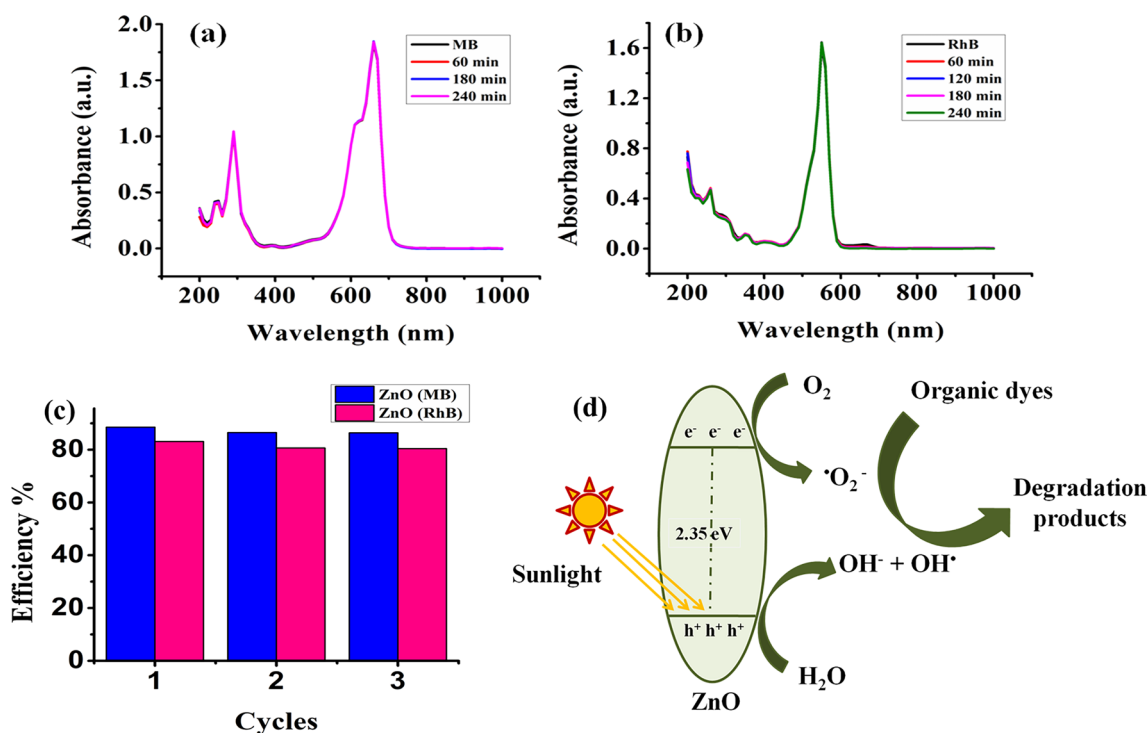


**Fig. 10** **a** UV–visible spectrum of MB dye samples at different time intervals in the presence of synthesized ZnO NPs under dark conditions and **b** UV–visible spectrum of RhB dye samples at different time intervals in the presence of synthesized ZnO NPs under

dark conditions. **c** Three cycles of photodegradation of MB dye and RhB dyes using ZnO nanoparticles under sunlight irradiation. **d** The plausible reaction mechanism for the photocatalytic degradation of organic dyes in the presence of as-synthesized ZnO NPs

nanoparticles degraded 88.53% of MB dye in the first cycle and 86.34% degradation of MB dye was observed in the third cycle. Also, synthesized ZnO nanoparticles degraded 83.08% of RhB dye in the first cycle and 80.38% degradation of RhB dye was observed in the third cycle. It can be seen that synthesized ZnO nanoparticles exhibited excellent reusability for photocatalytic degradation of MB dye and RhB under sunlight exposure for up to three cycles.

The probable reaction mechanism for the photocatalytic degradation of organic dyes in the presence of as-synthesized ZnO NPs is given in Fig. 10d. The plausible mechanism for the photocatalytic degradation of organic dyes is the formation of electron–hole pairs on the surface of ZnO NPs under sunlight irradiation. Generally, the hole from the valence band reacts with the H<sub>2</sub>O molecule to generate OH<sup>−</sup> anion and OH<sup>•</sup> radical. Also, the electron from the conduction band reacts with O<sub>2</sub> to generate O<sub>2</sub><sup>−•</sup> radical. All the OH<sup>•</sup>, OH<sup>−</sup>, and O<sub>2</sub><sup>−•</sup> are highly reactive and react with organic dye molecules adsorbed on the surface of synthesized ZnO NPs to generate degradation products (Yadav et al. 2022a, b).

Photocatalytic degradation behavior depends on the size and morphology of nanoparticles-based photocatalysts. Generally, photocatalytic activity increases with a decrease in the size of the nanoparticles due to an increase in surface area as well as available surface active sites which are mainly responsible for dye adsorption. In addition, the band gap of photocatalysts is also responsible for photocatalytic degradation behavior. ZnO-based semiconductor has some limitations for photocatalytic degradation application because of their wider band gap (~ 3.37 eV) which is responsible for the rapid recombination of electron–hole pair and absorption ability of only 5% of sunlight radiation (only UV region > 380 nm) (Karthik et al. 2022). Herein, the band gap of biosynthesized ZnO NPs

is reduced to 2.35 eV to overcome the above problems and thus as-synthesized ZnO NPs showed good photocatalytic degradation activities against MB and RhB organic dyes under sunlight irradiation. A comparative photocatalytic organic dye degradation activity of as-synthesized ZnO NPs with reported green synthesized ZnO nanomaterials is provided in Table 6.

## Conclusions

Flake-shaped ZnO NPs (P3) have been successfully prepared via green synthesis using the fruit peel extract of *Azadirachta indica* and then they are systematically evaluated as antimicrobial agents, supercapacitors, and photocatalysts. As-synthesized ZnO NPs showed higher antimicrobial activity against the gram-positive microbes (as a lower MIC value of 130 µg/mL determined for both *Staphylococcus aureus* and *Streptococcus pneumoniae*) than the gram-negative microbes (as a higher MIC value of 140 µg/mL and 135 µg/mL observed for *Pseudomonas aeruginosa* and *Escherichia coli*, respectively). Moreover, as-prepared ZnO NPs showed high specific capacitance and energy density values of 794.96 F/g and 22.3392 Wh/Kg, respectively, at 5 mV/s in 2 M KOH electrolyte and thus exhibited improved electrochemical performance as supercapacitor electrode material. Furthermore, as-synthesized ZnO NPs revealed photocatalytic degradation of 88.53% and 83.08% for the MB and RhB organic dyes, respectively, under 240 min of sunlight irradiation. In conclusion, as-prepared green synthesized flake-shaped ZnO NPs have great potential to be used as antimicrobial agents, photocatalysts for organic dye degradation, and electrode materials for supercapacitor applications.

**Table 6** A comparison of as-synthesized ZnO NPs with previously reported ZnO NPs based photocatalysts for organic dye degradation

S. no.	Photocatalysts	Plant extract used for biosynthesis	Light Source/ time of irradiation	Dye degradation efficiency %	References
1	ZnO nanoparticles	<i>Piper longum</i>	UV light/250 min	MB (69%)	Asha et al. (2022)
2	ZnO/bentonite nanocomposite	<i>Jujube</i> fruits extract	Sunlight/240 min	MB (97%)	Golmohammadi et al. (2022)
3	Cu-doped-ZnO nanoparticles	<i>Synadenium grantii</i> leaves extract	UV light/75 min	MB (79%) and RhB (75%)	Imade et al. (2022)
4	ZnO nanoparticles	<i>Syzygium cumini</i> leaves extract	Sunlight/180 min	MB (91%)	Sadiq et al. (2021)
5	ZnO nanoparticles	<i>Alchemilla vulgaris</i> leaves extract	UV light/120 min	RhB (75%)	Rajendrachari et al. (2021)
6	ZnO nanoparticles	<i>Acalypha indica</i> leaves extract	Sunlight/90 min	MB (96%)	Kamarajan et al. (2022)
7	ZnO nanoparticles	<i>Azadirachta indica</i> fruit peels extract	Sunlight/240 min	MB (88.53%) and RhB (83.08%)	This work

**Supplementary Information** The online version contains supplementary material available at <https://doi.org/10.1007/s11696-024-03340-6>.

**Acknowledgements** Kalawati Saini thanks Principal, Miranda House, University of Delhi for providing a laboratory to carry out the research work. The authors also thank USIC, University of Delhi, India for getting FE-SEM, EDS, and PXRD facilities. Kalawati Saini and Mona Saini thankful to DBT, GOVT. of India, New Delhi for providing fund (Ref. No. BT/IN/Indo/Foldscope/39/2015 dated: 20.03.2018). Sapna Yadav is grateful to CSIR, New Delhi for providing SRF (Ref. No. 08/700(0004)/2019-EMR-1). Kalawati Saini is grateful to Dr. Amrita Tripathi Sheikh, Associate Professor, Miranda House, University of Delhi for her constant encouragement and support.

## Declarations

**Conflict of interest** The authors declare no conflict of interest.

## References

- Akhavan O (2010) Graphene nanomesh by ZnO nanorod photocatalysts. *ACS Nano* 4(7):4174–4180. <https://doi.org/10.1021/nn1007429>
- Akhavan O, Ghaderi E (2010) Toxicity of graphene and graphene oxide nanowalls against bacteria. *ACS Nano* 4(10):5731–5736. <https://doi.org/10.1021/nn101390x>
- Akhavan O, Mehrabian M, Mirabbaszadeh K et al (2009) Hydrothermal synthesis of ZnO nanorod arrays for photocatalytic inactivation of bacteria. *J Phys D Appl Phys* 42(22):225305. <https://doi.org/10.1088/0022-3727/42/22/225305>
- Akhavan O, Ghaderi E, Esfandiari A (2011) Wrapping bacteria by graphene nanosheets for isolation from environment, reactivation by sonication, and inactivation by near-infrared irradiation. *J Phys Chem B* 115(19):6279–6288. <https://doi.org/10.1021/jp200686k>
- Alotaibi B, Negm WA, Elekhaway E et al (2022) Antibacterial activity of nano zinc oxide green-synthesized from *Gardenia thailandica* triveng. Leaves against *Pseudomonas aeruginosa* clinical isolates: in vitro and in vivo study. *Artif Cells Nanomed Biotechnol* 50(1):96–106. <https://doi.org/10.1080/21691401.2022.2056191>
- Arvanag FM, Bayrami A, Yangjeh AH et al (2019) A comprehensive study on antidiabetic and antibacterial activities of ZnO nanoparticles biosynthesized using *Silybum marianum* L. seed extract. *Mater Sci Eng C* 97:397–405. <https://doi.org/10.1016/j.msec.2018.12>
- Asha S, Bessy TC, Sherin JFJ et al (2022) Efficient photocatalytic degradation of industrial contaminants by *Piper longum* mediated ZnO nanoparticles. *Environ Res* 208:112686. <https://doi.org/10.1016/j.envres.2022.112686>
- Bala N, Saha S, Chakraborty M et al (2015) Green synthesis of zinc oxide nanoparticles using *Hibiscus subdariffa* leaf extract: effect of temperature on synthesis, anti-bacterial activity and anti-diabetic activity. *RSC Adv* 5:4993–5003. <https://doi.org/10.1039/C4RA12784F>
- Basri HH, Talib RA, Sukor R et al (2020) Effect of synthesis temperature on the size of ZnO nanoparticles derived from pineapple peel extract and antibacterial activity of ZnO–starch nanocomposite films. *Nanomaterials* 10(6):1061. <https://doi.org/10.3390/nano10061061>
- Becheri A, Durr M, Nostro PL et al (2008) Synthesis and characterization of zinc oxide nanoparticles: application to textiles as UV-absorbers. *J Nanopart Res* 10:679–689. <https://doi.org/10.1007/s11051-007-9318-3>
- Bijanazad K, Tadjarodi A, Akhavan O (2015) Photocatalytic activity of mesoporous microbricks of ZnO nanoparticles prepared by the thermal decomposition of bis (2-aminonicotinato) zinc (II). *Chin J Catal* 36(5):742–749. [https://doi.org/10.1016/S1872-2067\(14\)60305-3](https://doi.org/10.1016/S1872-2067(14)60305-3)
- Buldu-Akturk M, Toufani M, Tufanic A et al (2022) ZnO and reduced graphene oxide electrodes for all-in-one supercapacitor devices. *Nanoscale* 14:3269. <https://doi.org/10.1039/d2nr00018k>
- Choubari MS, Mazloom J, Ghodsi FE (2022) Supercapacitive properties, optical band gap, and photoluminescence of CeO<sub>2</sub>–ZnO nanocomposites prepared by eco-friendly green and citrate sol-gel methods: a comparative study. *Ceram Int* 48:21344–21354. <https://doi.org/10.1016/j.ceramint.2022.04.100>
- Djurišić AB, Choy WC, Roy VAL et al (2004) Photoluminescence and electron paramagnetic resonance of ZnO tetrapod structures. *Adv Funct Mater* 14(9):856–864. <https://doi.org/10.1002/adfm.200305082>
- Dobrucka R, Dugaszewsk J (2016) Biosynthesis and antibacterial activity of ZnO nanoparticles using *Trifolium pratense* flower extract. *Saudi J Biol Sci* 23:517–523. <https://doi.org/10.1016/j.sjbs.2015.05.016>
- Ehsani A, Bigdeloo M, Alamgholiloo H et al (2022) Ternary nanocomposite of TiO<sub>2</sub>–ZnO/MCM-41: synthesis and electrochemical performance in supercapacitors. *J Energy Storage* 50:104633. <https://doi.org/10.1016/j.est.2022.104633>
- Elumalai K, Velmurugan S (2015) Green synthesis, characterization and antimicrobial activities of zinc oxide nanoparticles from the leaf extract of *Azadirachta indica* (L.). *Appl Surf Sci* 345:329–336. <https://doi.org/10.1016/j.apsusc.2015.03.176>
- Elumalai K, Velmurugan S, Ravi S et al (2015) Bio-fabrication of zinc oxide nanoparticles using leaf extract of curry leaf (*Murraya koenigii*) and its antimicrobial activities. *Mater Sci Semicond Process* 34:365–372. <https://doi.org/10.1016/j.mssp.2015.01.048>
- Fouladi-Fard R, Aali R, Mohammadi-Aghdam S et al (2022) The surface modification of spherical ZnO with Ag nanoparticles: a novel agent, biogenic synthesis, catalytic and antibacterial activities. *Arab J Chem* 15:103658. <https://doi.org/10.1016/j.arabjc.2021.103658>
- Garcia L (2010) Broth microdilution MIC test. In: *Clinical microbiology procedures handbook*, 3rd edition. ASM Press, Washington, DC, pp 25–41. <https://doi.org/10.1128/9781555817435.ch5.2>
- Golmohammadi M, Honarmand M, Esmaeili A (2022) Biosynthesis of ZnO nanoparticles supported on bentonite and the evaluation of its photocatalytic activity. *Mater Res Bull* 149:111714. <https://doi.org/10.1016/j.materresbull.2021.111714>
- Hamed R, Sawalha S, Assali M et al (2023) Visible light-driven ZnO nanoparticles/carbon nanodots hybrid for broad-spectrum antimicrobial activity. *Surf Interfaces* 38:102760. <https://doi.org/10.1016/j.surfin.2023.102760>
- Handayani M, Mulyaningsih Y, Anggoro MA et al (2022) One-pot synthesis of reduced graphene oxide/chitosan/zinc oxide ternary nanocomposites for supercapacitor electrodes with enhanced electrochemical properties. *Mater Lett* 314:131846. <https://doi.org/10.1016/j.matlet.2022.131846>
- Harun K, Hussain F, Purwanto A et al (2017) Sol–gel synthesized ZnO for optoelectronics applications: a characterization review. *Mater Res Express* 4(12):122001. <https://doi.org/10.1088/2053-1591/aa9e82>
- Huang Z, Zheng X, Yan D et al (2008) Toxicological effect of ZnO nanoparticles based on bacteria. *Langmuir* 24(8):4140–4144. <https://doi.org/10.1021/la703594g>
- Ibrahim OH, Mousa MA, Asiry KA et al (2022) *Azadirachta indica* A. juss fruit mesocarp and epicarp extracts induce antimicrobial and antiproliferative effects against prostate (PC-3), Breast (MCF-7), and colorectal adenocarcinoma (Caco-2) cancer cell lines through

- upregulation of proapoptotic genes. *Plants* 11(15):1990. <https://doi.org/10.3390/plants11151990>
- Imade EE, Ajiboye TO, Fadji AE et al (2022) Green synthesis of zinc oxide nanoparticles using plantain peel extracts and the evaluation of their antibacterial activity. *Sci Afr* 16:e01152. <https://doi.org/10.1016/j.sciaf.2022.e01152>
- Irimpan L, Nampoori VPN, Radhakrishnan P et al (2007) Size dependent fluorescence spectroscopy of nanocolloids of ZnO. *J Appl Phys* 102(6):063524. <https://doi.org/10.1063/1.2778637>
- Jannesari M, Akhavan O, Madaah Hosseini HR et al (2020) Graphene/CuO<sub>2</sub> nanoshuttles with controllable release of oxygen nanobubbles promoting interruption of bacterial respiration. *ACS Appl Mater Interfaces* 12(32):35813–35825. <https://doi.org/10.1021/acsami.0c05732>
- Jannesari M, Akhavan O, Hosseini HRM et al (2023) Oxygen-rich graphene/ZnO<sub>2</sub>-Ag nanoframeworks with pH-switchable catalase/peroxidase activity as O<sub>2</sub> nanobubble-self generator for bacterial inactivation. *J Colloid Interface Sci* 637:237–250. <https://doi.org/10.1016/j.jcis.2023.01.079>
- Jayaseelan C, Rahumana AA, Kirthi A et al (2012) Novel microbial route to synthesize ZnO nanoparticles using *Aeromonas hydrophila* and their activity against pathogenic bacteria and fungi. *Spectrochim Acta A Mol Biomol Spectro* 90:78–84. <https://doi.org/10.1016/j.saa.2012.01.006>
- Ji X, Wang A, Li G et al (2016) Controllable synthesis and photocatalytic properties of ZnO hierarchical flower-like porous nanostructures. *Micro Nano Lett* 11(11):753–757. <https://doi.org/10.1049/mnl.2016.0404>
- Jones N, Ray B, Ranjit KT et al (2008) Antibacterial activity of ZnO nanoparticle suspensions on a broad spectrum of microorganisms. *FEMS Microb Lett* 279(1):71–76. <https://doi.org/10.1111/j.1574-6968.2007.01012.x>
- Kamarajan G, Anburaj DB, Porkalai V et al (2022) Green synthesis of ZnO nanoparticles and their photocatalyst degradation and antibacterial activity. *J Water Environ Nanotechnol* 7(2):180–193. <https://doi.org/10.22090/jwent.2022.02.006>
- Kandasamy G, Soni S, Sushmita K et al (2019) One-step synthesis of hydrophilic functionalized and cytocompatible SPIONs based aqueous ferrofluids for biomedical applications. *J Mol Liq* 274:653–663. <https://doi.org/10.1016/j.molliq.2018.10.161>
- Karthik KV, Raghu AV, Reddy KR et al (2022) Green synthesis of Cu-doped ZnO nanoparticles and its application for the photocatalytic degradation of hazardous organic pollutants. *Chemosphere* 287:132081. <https://doi.org/10.1016/j.chemosphere.2021.132081>
- Khan M, Ware P, Shimpi N (2021) Synthesis of ZnO nanoparticles using peels of *Passiflora foetida* and study of its activity as an efficient catalyst for the degradation of hazardous organic dye. *SN Appl Sci* 3:528. <https://doi.org/10.1007/s42452-021-04436-4>
- Khara G, Padalia H, Moteriya P et al (2018) *Peltophorum pterocarpum* flower-mediated synthesis, characterization, antimicrobial and cytotoxic activities of ZnO nanoparticles. *Arab J Sci Eng* 43:3393–3401. <https://doi.org/10.1007/s13369-017-2875-6>
- Kilani-Morakchi S, Morakchi-Goudjil H, Sifi K (2021) Azadirachtin-based insecticide: overview, risk assessments, and future directions. *Front Agron* 3:676208. <https://doi.org/10.3389/fagro.2021.676208>
- Koumaglo K, Akogo Y, Dotse K et al (2004) Évaluation de la teneur en gédunine dans différents organes d'*Azadirachta indica* A. Juss C R Chim 7:1047–1050. <https://doi.org/10.1016/j.crci.2003.12.032>
- Kumar A, Pandey AK, Singh SS et al (2011) Engineered ZnO and TiO<sub>2</sub> nanoparticles induce oxidative stress and DNA damage leading to reduced viability of *Escherichia coli*. *Free Radic Biol Med* 51(10):1872–1881. <https://doi.org/10.1016/j.freeradbiomed.2011.08.025>
- Li J, Li Y, Wu H et al (2021) Facile synthesis of ZnO nanoparticles by *Actinidia deliciosa* fruit peel extract: bactericidal, anticancer and detoxification properties. *Environ Res* 200:111433. <https://doi.org/10.1016/j.envres.2021.111433>
- Liang Y, Guo N, Li L et al (2015) Preparation of porous 3D Cd-doped ZnO microflowers with enhanced photocatalytic performance. *RSC Adv* 5:59887. <https://doi.org/10.1039/c5ra08519e>
- Liu S, Zeng TH, Hofmann M et al (2011) Antibacterial activity of graphite, graphite oxide, graphene oxide, and reduced graphene oxide: membrane and oxidative stress. *ACS Nano* 5(9):6971–6980. <https://doi.org/10.1021/nn202451x>
- Madan HR, Sharma SC, Udayabhanu et al (2016) Facile green fabrication of nanostructure ZnO plates, bullets, flower, prismatic tip, closed pine cone: their antibacterial, antioxidant, photoluminescent and photocatalytic properties. *Spectrochim Acta A Mol Biomol Spectrosc* 152:404–416. <https://doi.org/10.1016/j.saa.2015.07.067>
- Maity D, Agrawal DC (2007) Synthesis of iron oxide nanoparticles under oxidizing environment and their stabilization in aqueous and non-aqueous media. *J Magn Magn Mater* 308(1):46–55. <https://doi.org/10.1016/j.jmmm.2006.05.001>
- Mashentseva AA, Aimanova NA, Parmanbek N et al (2022) *Serratula coronata* L. mediated synthesis of ZnO nanoparticles and their application for the removal of Alizarin yellow R by photocatalytic degradation and adsorption. *Nanomaterials* 12:3293. <https://doi.org/10.3390/nano12193293>
- Moghadam MTT, Seif M (2022) Fabrication and investigation of ZnO-CNT@Fe<sub>3</sub>O<sub>4</sub>/NF as supercapacitor electrode by using a novel preparation method of CNT. *Diam Relat Mater* 125:108962. <https://doi.org/10.1016/j.diamond.2022.108962>
- Mohammadi-Aloucheh R, Habibi-Yangjeh A, Bayrami A et al (2018) Green synthesis of ZnO and ZnO/CuO nanocomposites in *Mentha longifolia* leaf extract: characterization and their application as anti-bacterial agents. *J Mater Sci Mater Electron* 29:13596–13605. <https://doi.org/10.1007/s10854-018-9487-0>
- Mohan A, Manikandan V, Devanesan S et al (2022) Nanostructured nickel doped zinc oxide material suitable for magnetic, supercapacitor applications and theoretical investigation. *Chemosphere* 299:134366. <https://doi.org/10.1016/j.chemosphere.2022.134366>
- Muniyan A, Ravi K, Mohan U et al (2017) Characterization and in vitro antibacterial activity of saponin-conjugated silver nanoparticles that cause burn wound infection. *World J Microbiol Biotechnol* 33(7):1–12. <https://doi.org/10.1007/s11274-017-2309-3>
- Nagarani S, Sasikala G, Yuvaraj M et al (2022) ZnO–CuO nanoparticles enamelled on reduced graphene nanosheets as electrode materials for supercapacitors applications. *J Energy Storage* 52:104969. <https://doi.org/10.1016/j.est.2022.104969>
- Nethaji P, Kumar PS (2022) V–Ag doped ZnO nanorod as high-performance electrode material for supercapacitors with enhanced specific capacitance and cycling stability. *Chem Eng Res Des* 178:356–368. <https://doi.org/10.1016/j.cherd.2021.12.039>
- Noohpisheha Z, Amiri H, Farhadi S et al (2020) Green synthesis of Ag–ZnO nanocomposites using *Trigonella foenum-graecum* leaf extract and their antibacterial, antifungal, antioxidant and photocatalytic properties. *Spectrochim Acta A Mol Biomol Spectrosc* 240:118595. <https://doi.org/10.1016/j.saa.2020.118595>
- Padalia H, Chanda S (2017) Characterization, antifungal and cytotoxic evaluation of green synthesized zinc oxide nanoparticles using *Ziziphus nummularia* leaf extract. *Artif Cells Nanomed Biotechnol* 45(8):1751–1761. <https://doi.org/10.1080/21691401.2017.1282868>
- Padalia H, Moteriya P, Chanda S (2018) Synergistic antimicrobial and cytotoxic potential of zinc oxide nanoparticles synthesized using *Cassia auriculata* leaf extract. *BioNanoScience* 8(1):196–206. <https://doi.org/10.1007/s12668-017-0463-6>
- Prasanna VL, Vijayaraghavan R (2015) Insight into the mechanism of antibacterial activity of ZnO: surface defects mediated reactive



- oxygen species even in the dark. *Langmuir* 31(33):9155–9162. <https://doi.org/10.1021/acs.langmuir.5b02266>
- Prashanth GK, Prashanth PA, Bora U et al (2015) In vitro antibacterial and cytotoxicity studies of ZnO nanopowders prepared by combustion assisted facile green synthesis. *Karbala Int J Mod Sci* 1:67–77. <https://doi.org/10.1016/j.kijoms.2015.10.007>
- Rabiee N, Akhavan O, Fatahi Y et al (2022) CaZnO-based nanoghosts for the detection of ssDNA, pCRISPR and recombinant SARS-CoV-2 spike antigen and targeted delivery of doxorubicin. *Chemosphere* 306:135578. <https://doi.org/10.1016/j.chemosphere.2022.135578>
- Rajendrachari S, Taslimi P, Karaoglanli AC et al (2021) Photocatalytic degradation of Rhodamine B (RhB) dye in waste water and enzymatic inhibition study using cauliflower shaped ZnO nanoparticles synthesized by a novel one-pot green synthesis method. *Arab J Chem* 14:103180. <https://doi.org/10.1016/j.arabjc.2021.103180>
- Ramesh M, Anbuvaran M, Viruthagiri G (2015) Green synthesis of ZnO nanoparticles using *Solanum nigrum* leaf extract and their antibacterial activity. *Spectrochim Acta a Mol Biomol Spectrosc* 136:864–870. <https://doi.org/10.1016/j.saa.2014.09.105>
- Rani N, Saini M, Yadav S et al (2020) High performance Supercapacitor based on rod shaped ZnO Nanostructure electrode. *AIP Conf Proc* 2276:020042. <https://doi.org/10.1063/5.0026084>
- Rani N, Goswami N, Maity D et al (2022a) Biosynthesis of hydrophilic Zinc oxide nanoparticles using *Plumeria Obtusa* and *Tabernaemontana divaricate* flower extract for antidiabetic treatment. *Chem Pap*. <https://doi.org/10.1007/s11696-022-02239-4>
- Rani N, Rawat K, Saini M et al (2022b) *Azadirachta indica* leaf extract mediated biosynthesized rod-shaped zinc oxide nanoparticles for in vitro lung cancer treatment. *Mater Sci Eng B* 284:115851. <https://doi.org/10.1016/j.mseb.2022.115851>
- Rani N, Rawat K, Saini M et al (2022c) Rod-shaped ZnO nanoparticles: synthesis, comparison and in vitro evaluation of their apoptotic activity in lung cancer cells. *Chem Pap* 76:1225–1238. <https://doi.org/10.1007/s11696-021-01942-y>
- Rani N, Rani S, Patel H et al (2023) Characterization and investigation of antioxidant and antimicrobial activity of zinc oxide nanoparticles prepared using leaves extract of *Nyctanthes arbor-tristis*. *Inorg Chem Commun* 150:110516. <https://doi.org/10.1016/j.inoche.2023.110516>
- Ray PG, Biswas S, Roy T et al (2019) Sonication assisted hierarchical decoration of Ag-NP on zinc oxide nanoflower impregnated egg-shell membrane: evaluation of antibacterial activity and in vitro cytocompatibility. *ACS Sustain Chem Eng* 7(16):13717–13733. <https://doi.org/10.1021/acssuschemeng.9b01185>
- Rokhsat E, Akhavan O (2016) Improving the photocatalytic activity of graphene oxide/ZnO nanorod films by UV irradiation. *Appl Surf Sci* 371:590–595. <https://doi.org/10.1016/j.apsusc.2016.02.222>
- Sadiq H, Sher F, Sehar S et al (2021) Green synthesis of ZnO nanoparticles from *Syzygium cumini* leaves extract with robust photocatalysis applications. *J Mol Liq* 335:116567. <https://doi.org/10.1016/j.molliq.2021.116567>
- Saini M, Mushtaq A, Yadav S et al (2022) Green synthesis of rod shaped ZnO using *Origanum majorana* leaf extract and their study for antibacterial applications. *IOP Conf Ser Mater Sci Eng* 1225:012048. <https://doi.org/10.1088/1757-899X/1225/1/012048>
- Saini M, Yadav S, Rani N et al (2022b) Antibacterial study of nano-sized zinc oxide (F1) against various gram-positive and gram-negative bacteria. *Mater Today Proc* 67(6):852–857. <https://doi.org/10.1016/j.matpr.2022.07.208>
- Saini M, Yadav S, Rani N et al (2022c) Biosynthesized zinc oxide nanoparticles using seed and bark extract of *Azadirachta indica* for antibacterial, photocatalytic and supercapacitor applications. *Mater Sci Eng B* 282:115789. <https://doi.org/10.1016/j.mseb.2022.115789>
- Sana SS, Kumbhakar DV, Pasha A et al (2020) *Crotalaria verrucosa* leaf extract mediated synthesis of zinc oxide nanoparticles: assessment of antimicrobial and anticancer activity. *Molecules* 25(21):4896. <https://doi.org/10.3390/molecules25214896>
- Sinha R, Roy N, Mandal TK (2022) SWCNT/ZnO nanocomposite decorated with carbon dots for photoresponsive supercapacitor applications. *Chem Eng J* 431:133915. <https://doi.org/10.1016/j.cej.2021.133915>
- Soltanian S, Sheikhabaei M, Mohamadi N et al (2021) Biosynthesis of zinc oxide nanoparticles using *Hertia intermedia* and evaluation of its cytotoxic and antimicrobial activities. *BioNanoScience* 11(2):245–255. <https://doi.org/10.1007/s12668-020-00816-z>
- Srivastava SK, Agrawal B, Kumar A et al (2020) Phytochemicals of *Azadirachta indica* source of active medicinal constituent used for cure of various diseases: a review. *J Sci Res* 64(1):385–390. <https://doi.org/10.37398/JSR.2020.640153>
- Subramanian H, Krishnan M, Mahalingam A (2022) Photocatalytic dye degradation and photoexcited anti-microbial activities of green zinc oxide nanoparticles synthesized via *Sargassum muticum* extracts. *RSC Adv* 12:985. <https://doi.org/10.1039/d1ra08196a>
- Umar A, Rahman MM, Al-Hajry A et al (2009) Highly-sensitive cholesterol biosensor based on well-crystallized flower-shaped ZnO nanostructures. *Talanta* 78:284–289. <https://doi.org/10.1016/j.talanta.2008.11.018>
- Velsankar K, Venkatesan A, Muthumari P et al (2022) Green inspired synthesis of ZnO nanoparticles and its characterizations with biofilm, antioxidant, anti-inflammatory, and anti-diabetic activities. *J Mol Struct* 1255:132420. <https://doi.org/10.1016/j.molstruc.2022.132420>
- Vijayakumar S, Vinoj G, Malaikozhundan B et al (2015) *Plectranthus amboinicus* leaf extract mediated synthesis of zinc oxide nanoparticles and its control of methicillin resistant *Staphylococcus aureus* biofilm and blood sucking mosquito larvae. *Spectrochim Acta A Mol Biomol Spectrosc* 137:886–891. <https://doi.org/10.1016/j.saa.2014.08.064>
- Vinayagam R, Sharma G, Murugesan G et al (2022) Rapid photocatalytic degradation of 2, 4-dichlorophenoxy acetic acid by ZnO nanoparticles synthesized using the leaf extract of *Muntingiacal-abura*. *J Mol Struct* 1263:133127. <https://doi.org/10.1016/j.molstruc.2022.133127>
- Visinescu D, Hussien MD, Moreno JC et al (2018) Zinc oxide spherical-shaped nanostructures: investigation of surface reactivity and interactions with microbial and mammalian cells. *Langmuir* 34(45):13638–13651. <https://doi.org/10.1021/acs.langmuir.8b02528>
- Wang YW, Cao A, Jiang Y et al (2014) Superior antibacterial activity of zinc oxide/graphene oxide composites originating from high zinc concentration localized around bacteria. *ACS Appl Mater Interfaces* 6(4):2791–2798. <https://doi.org/10.1021/am4053317>
- Yadav S, Rani N, Saini K (2022a) Green synthesis of ZnO and CuO NPs using *Ficus benghalensis* leaf extract and their comparative study for electrode materials for high performance supercapacitor application. *Mater Today Proc* 49:2124–2130. <https://doi.org/10.1016/j.matpr.2021.08.323>
- Yadav S, Yadav J, Kumar M et al (2022b) Synthesis and characterization of nickel oxide/cobalt oxide nanocomposite for effective degradation of methylene blue and their comparative electrochemical study as electrode material for supercapacitor application. *Int J Hydrog Energy* 47:41684–41697. <https://doi.org/10.1016/j.ijhydene.2022.02.011>
- Yadav S, Rani N, Saini K (2023a) Coupling ZnO with CuO for efficient organic pollutant removal. *Environ Sci Pollut Res* 30:71984–72008. <https://doi.org/10.1007/s11356-022-24139-6>
- Yadav S, Shakya K, Gupta A et al (2023b) A review on degradation of organic dyes by using metal oxide semiconductors.

Environ Sci Pollut Res 30:71912–71932. <https://doi.org/10.1007/s11356-022-20818-6>

Yadav S, Rani N, Saini K (2023c) Synthesis and characterization of NiO/Cr<sub>2</sub>O<sub>3</sub> nanocomposite with effective sunlight driven photocatalytic degradation of organic dyes. Environ Sci Pollut Res 30:71957–71969. <https://doi.org/10.1007/s11356-022-22746-x>

**Publisher's Note** Springer Nature remains neutral with regard to jurisdictional claims in published maps and institutional affiliations.

## Authors and Affiliations

Nutan Rani<sup>1</sup> · Sapna Yadav<sup>1</sup> · Asifa Mushtaq<sup>2</sup> · Swati Rani<sup>3</sup> · Mona Saini<sup>1</sup> · Seema Rawat<sup>4</sup> · Kalpna Gupta<sup>5</sup> · Kalawati Saini<sup>1</sup>  · Dipak Maity<sup>6</sup>

✉ Kalawati Saini  
kalawati.saini@mirandahouse.ac.in

✉ Dipak Maity  
dipakmaity@gmail.com

<sup>1</sup> Department of Chemistry, Miranda House, University of Delhi, Patel Chest Marg, New Delhi 110007, India

<sup>2</sup> Department of Botany and Microbiology, H.N.B. Garhwal University, Srinagar, Uttarakhand 241674, India

Springer Nature or its licensor (e.g. a society or other partner) holds exclusive rights to this article under a publishing agreement with the author(s) or other rightsholder(s); author self-archiving of the accepted manuscript version of this article is solely governed by the terms of such publishing agreement and applicable law.

<sup>3</sup> Department of Chemistry, University of Delhi, Delhi 110007, India

<sup>4</sup> School of Life Sciences, Central University of Gujarat, Sector-30, Gandhinagar, Gujarat 382030, India

<sup>5</sup> Department of Chemistry, Raj Rishi Government College, Alwar, Rajasthan 301001, India

<sup>6</sup> School of Public Health, Texas A&M University, College Station TX 77843, United States of America